arXiv:1507.02980v1 [math.CA] 7 Jul 2015

A HYBRID MATHEMATICAL MODEL OF COLLECTIVE MOTION UNDER ALIGNMENT AND CHEMOTAXIS

EZIO DI COSTANZO[1] AND ROBERTO NATALINI[2]

Abstract. In this paper we propose and study a hybrid *discrete in continuous* mathematical model of collective motion under alignment and chemotaxis effect. Starting from the paper by Di Costanzo et al (2015), in which the Cucker-Smale model (Cucker and Smale, 2007) was coupled with other cell mechanisms, to describe the cell migration and self-organization in the zebrafish lateral line primordium, we introduce a simplified model in which the coupling between an alignment and chemotaxis mechanism acts on a system of interacting particles. In particular we rely on a hybrid description in which the agents are discrete entities, while the chemoattractant is considered as a continuous signal. The proposed model is then studied both from an analytical and a numerical point of view. From the analytic point of view we prove, globally in time, existence and uniqueness of the solution. Then, the asymptotic behaviour of the system is investigated. Through a suitable Lyapunov functional we show that, for the linearized version of our system, for $t \to +\infty$, the migrating aggregate exponentially converge to a state in which all the particles have a same position with zero velocity. Finally, from the numerical point of view, some meaningful dynamical tests are proposed to simulate the behaviour of the system, also in comparison with the analytical findings.

1. Introduction

A collective motion is a form of collective behaviour in which the individual unit's action is strongly dominated by the influence of other units, so that its motion results very different from how it would be if it was alone. Collective motion has been extensively studied in recent year in a great variety of systems, from non-living systems, such as nematic fluids, nano swimmers, simple robots, to living systems, such as bacteria colonies, cell aggregates, swarms of insects, flocks of birds, schools of fish, swarms of insects, herds of mammals, crowds of humans. Many references can be found, for example, in the review by Vicsek and Zafeiris (2012).

Different reasons of aggregations in a given system have been proposed. Coordinated motion of cells results in making a biological process more efficient (e.g. in embryogenesis, wound healing, immune response, etc.), while in the case of tumour cell invasion it appears to speed up the progression of the decease (Méhes and Vicsek, 2014). For the animals entities it is observed that a group can more efficiently explore surrounding environments, to enhance foraging capability and detection of predators (Pitcher et al, 1982); being in a group offers protection

---

[1] Istituto per le Applicazioni del Calcolo "M. Picone" – Consiglio Nazionale delle Ricerche, Via Pietro Castellino 111, 80131 Naples, Italy.

[2] Istituto per le Applicazioni del Calcolo "M. Picone" – Consiglio Nazionale delle Ricerche, Via dei Taurini 19, 00185 Rome, Italy.

E-mail addresses: [1]`e.dicostanzo@na.iac.cnr.it`, [2]`roberto.natalini@cnr.it`.

2010 *Mathematics Subject Classification.* 82C22, 34D05, 92C17.

Key words and phrases. Differential equations, existence and uniqueness of solution, asymptotic stability, Lyapunov function, collective motion, Cucker-Smale model, flocking behaviour, chemotaxis, self-organization, finite differences.

against attacks by predators (Ioannou et al, 2008) and increases the locomotion efficiency (Fish, 1995).

The research in the field of collective motion modelling is of great interest for the applications in many fields of the real life, from biomedical field, e.g. in relation to the collective motion of cells (see Szabò et al, 2006; Belmonte et al, 2008; Arboleda-Estudillo et al, 2010; Sepúlveda et al, 2013; Joie et al, 2013; Colin et al, 2013; Di Costanzo et al, 2015; and the reviews by Hatzikirou and Deutsch, 2007 and Méhes and Vicsek, 2014), to socio-economic field and life sciences (Naldi et al, 2010; Pareschi and Toscani, 2014), to the problems of pedestrian flows (Helbing et al, 1997; Piccoli and Tosin, 2009; Faria et al, 2010; Cristiani et al, 2010; Bruno et al, 2011; Moussaïd et al, 2011; Cristiani et al, 2014, 2015).

Basic mathematical models about collective motion are substantially based on one or more of the following steering behaviours of the units: *alignment*, in order to move in the same direction of average heading direction of neighbouring units (Vicsek et al, 1995; Cucker and Smale, 2007, and references therein); *separation*, in order to avoid crowding, and *cohesion*, to remain close to the average position of neighbours (D'Orsogna et al, 2006; Strömbom, 2011). Sometimes *three-zone models* combine together alignment, attraction and repulsion effects on three non-overlapping regions, which take into account the sensory capabilities of the individual (Aoki, 1982; Couzin et al, 2002; Grégoire et al, 2003; Grégoire and Chaté, 2004). For example, the visual field of a bird does not extend behind its body, fishes can accompany visual signals with those coming from their lateral line, while cells can feel stimuli around them. This leads to introduce the concept of the *cone of vision* (Huth and Wissel, 1992; Couzin et al, 2002; Hemelrijk and Hildenbrandt, 2008). In general the cone of interaction is not only animal-dependent, but it can also vary depending on the type of motion, environmental conditions, presence of predators, and aim of the displacement (Cristiani et al, 2011). Moreover, when each unit interacts only with those particles which are closer than a predefined distance, that is a fixed range of influence, we speak about "metric" interaction. On the other hand, recent studies of starling flocks, on the other hand, have shown that each bird modifies its position relative to the mates directly surrounding it (typically six or seven individuals), no matter how close or how far away those animals are. In this type of behaviour, referred as "topological" interaction (Ballerini et al, 2008), the radius of perception is adjusted by each individual, in such way that the neighbourhood of interaction encompasses a predefined mass of other individuals felt comfortable to interact with it (Cristiani et al, 2010; Cristiani et al, 2011, and references therein).

With regard to the alignment models a widespread model is represented by the Cucker-Smale model (Cucker and Smale, 2007). The original model was proposed to describe the dynamics in a flock of birds, but its applicability is to general phenomena where autonomous agents reach a consensus, e.g. animal herding, emergence of common languages in primitive societies, etc. (Couzin et al, 2005). The starting point of this model is represented by the seminal paper by Vicsek et al (1995) and previous analytic studies can be found also in Tsitsiklis (1984) and Jadbabaie et al (2003). Anyway, the Cucker-Smale paper is widely known to have established an analytical exact result on the convergence to the same velocity in a group of interacting agents through an alignment effect.

The hypothesis of the Cucker-Smale model is that the force acting on every particle (bird) is a weighted average of the differences of its velocity with those of the other particles (birds). In particular, for $N \in \mathbb{N}$ particles, the proposed model, in continuous time $t \in \mathbb{R}_{\geq 0}$, can be written in the form

$$\begin{cases} \dot{\mathbf{V}}_i = \dfrac{1}{N} \displaystyle\sum_{j=1}^{N} \dfrac{\alpha_1}{\Big(\alpha_2 + \|\mathbf{X}_i - \mathbf{X}_j\|^2\Big)^{\sigma}} (\mathbf{V}_j - \mathbf{V}_i), \\ \dot{\mathbf{X}}_i = \mathbf{V}_i, \end{cases} \tag{1.1}$$

where $\mathbf{X}_i, \mathbf{V}_i \in \mathbb{R}^n$, for $i = 1, \dots, N$, are the position and the velocity of the i-th particle, α_1, α_2, σ are positive constants and $\|\cdot\|$ is the Euclidean norm in $\mathbb{R}^n$. In particular σ captures the rate of decay of the influence between agents in the flock as they separate in space, and it is a fundamental parameter in the time-asymptotic behaviour of system (1.1) (see below). In particular, under suitable initial data and parameters the model implies that the state of the group converges to one in which all particles move with the same velocity, said *flocking state*.

The main convergence result proved in Cucker and Smale (2007) has been improved by Ha and Liu (2009), using an explicit Lyapunov functional approach. First, as in this last reference, we can give the definition of *time-asymptotic flocking* as follows:

Definition 1. *Given system* (1.1)*, let* $\mathbf{X}_{CM} = \frac{1}{N}\sum_{i=1}^{N} \mathbf{X}_i$ *and* $\mathbf{V}_{CM} = \frac{1}{N}\sum_{i=1}^{N} \mathbf{V}_i$ *position and velocity of the centre of mass. System* (1.1) *has a time-asymptotic flocking if and only if* $(\mathbf{X}_i, \mathbf{V}_i)$*,* $i = 1, \dots, N$*, satisfy the two conditions:*

1) the velocity fluctuations go to zero time-asymptotically (velocity alignment):

$$\lim_{t \to +\infty} \sum_{i=1}^{N} \|\mathbf{V}_i(t) - \mathbf{V}_{CM}(t)\|^2 = 0; \tag{1.2}$$

2) the position fluctuations are uniformly bounded in time t *(forming a group):*

$$\sup_{0 \le t \le +\infty} \sum_{i=1}^{N} \|\mathbf{X}_i(t) - \mathbf{X}_{CM}(t)\|^2 < +\infty. \tag{1.3}$$

Notice that the square root of the quantities under the limit and supremum operations in (1.2)–(1.3) is proportional to the standard deviations of $\mathbf{V}_i(t)$ and $\mathbf{X}_i(t)$ around the centre of mass system. Cucker and Smale (2007) and Ha and Liu (2009) proved that for $\sigma \in [0, 1/2]$ occurs a global *unconditional flocking* of system (1.1), as stated in Definition 1, regardless of initial configurations, while for $\sigma \in (1/2, +\infty)$ there is *conditional flocking*, that is only some parameters and initial data lead to a flocking state, but in general the dispersion of the flock may occur.

Cucker and Smale-like models have been widely employed in collective dynamics and several applications can be found, from the biological field (Szabò et al, 2006; Belmonte et al, 2008; Arboleda-Estudillo et al, 2010; Sepúlveda et al, 2013; Di Costanzo et al, 2015), to the collective motion of different interacting groups (Albi and Pareschi, 2013). Furthermore, many extensions have been proposed. For example, Cucker and Dong (2010, 2011) added a repelling force between particles in equation $(1.1)_1$, proving an analogous convergence theorem ensuring, on certain conditions, flocking behaviour, in addition without collision between particles. Ha and Levy (2009) applied system (1.1) to describe the motion of phototactic bacteria (i.e., bacteria that move towards light), adding a force that move excited bacteria towards the light source in equation $(1.1)_1$, and an additional equation for the excitation level of each particle. Also in this case, under particular conditions, it is proved that the asymptotic velocity of the particles tends to an identical terminal velocity. Other models have introduced noise (Cucker and Mordecki, 2008), stochastic equations (Ha et al, 2009), leader individuals with a preferred heading direction (Cucker and Huepe, 2008), kinetic equations (Carrillo et al, 2010).

In this paper, starting from the model proposed by Di Costanzo et al (2015) in relation to the morphogenesis in the zebrafish lateral line primordium, in which the authors coupled the Cucker-Smale model with other cell mechanisms (chemotaxis, attraction-repulsion, damping effects), we study, both from an analytical and a numerical point of view, a simplified model in which the coupling between an alignment and chemotaxis effect acts in a system of interacting particles. Our description is hybrid: discrete for the interacting agents, and continuous for the chemotactic signal. From the analytic point of view, in the two-dimensional case with N particles, we prove, globally in time, existence and uniqueness of solution of the model. Then, the time-asymptotic behaviour of the model is investigated on a linearized version of the system. In particular, through a suitable Lyapunov functional, is shown that position and velocity of all the particles go exponentially to those of their centre of mass. Moreover, the velocity of the centre of mass tends time-asymptotically to zero. From a numerical point of view, on a bounded domain with periodic boundary conditions, some 2D dynamical tests are proposed to simulate the behaviour of the full nonlinear model, and to compare the numerical results with those analytical.

From our findings, we observe that while in the Cucker-Smale model two conditions may occur, conditional and unconditional flocking, in our model the flocking behaviour, as given in Definition 1, is always ensured. Moreover, we have the stronger conditions that all the particles converge in a single position, i.e. their centre of mass, and that the velocity of the centre of mass tends to zero.

Among the various numerical simulations, we discuss the competition between alignment and chemotactic effects varying the parameters of the system. We find a decrease in the rate of convergence of the particles when the strength of the alignment term increases with respect to the chemotaxis. On the other hand, an increase in the rate of convergence can be found with the same parameters and with a greater number of interacting particles. Inspired then from the aforesaid paper on the zebrafish lateral line, we consider also the case of two kinds of cells: leader cells corresponding to the sources of the chemotactic signal, and follower cells that do not produce any chemical signal, both subject to the alignment and chemotaxis force. In this case we observe the convergence of the group toward the sources of the chemoattractant. Finally, we consider the collective motion under chemotaxis, neglecting the alignment effect. Our numerical tests, in this regard, show the absence of convergence, and an oscillating motion of the particles around their centre of mass. This suggests that, in such model, the only chemotactic effect is unable to reproduce biological phenomena involving stationary aggregates.

The paper is organized as follows. In Section 2 we design our hybrid mathematical model of collective motion. Section 3 deals with the analytical study of the local existence and uniqueness of the solution. Then, in Section 4 this result is extended and the global existence and uniqueness is proved. Section 5 is devoted to investigate the asymptotic behaviour of the model around the equilibrium configurations. In Section 6 we show and discuss some meaningful dynamical simulations of the model. Finally, Section 7 includes the conclusions and possible future perspectives.

2. The basic mathematical model

Starting from model (1.1), we suppose that the force acting on each particle is given by an alignment term, proportional to the differences of velocity with the other particles and weighed on the distances, and by a chemotactic attraction towards higher concentration of a chemical signal $f(\mathbf{x},t)$, supposed produced by the particles themselves. Typically, this last force is proportional to the gradient of the concentration ∇f (see Eisenbach and Lengeler, 2004 for biological backgrounds, and Murray, 2003; Perthame, 2007 for some mathematical references). In our hybrid description, while particles are considered discrete entities, the signal f is supposed to be continuous and its rate of change in time is equal to a diffusion term, a source term, and a molecular degradation. If each particles is endowed of a radius R, describing its circular shape, the source of signal can be given by a characteristic function on a ball of radius R centred on each particle.

To summarize our hypotheses, we write the following system:

$$\begin{cases} \dot{\mathbf{V}}_i = \dfrac{\beta}{N}\displaystyle\sum_{j=1}^{N} \frac{1}{\left(1+\frac{\|\mathbf{X}_i-\mathbf{X}_j\|^2}{R^2}\right)^{\sigma}}(\mathbf{V}_j-\mathbf{V}_i)+\gamma\nabla f(\mathbf{X}_i), \\ \\ \dot{\mathbf{X}}_i = \mathbf{V}_i, \\ \\ \partial_t f = D\Delta f + \xi\displaystyle\sum_{j=1}^{N}\chi_{\mathbf{B}(\mathbf{X}_j,R)} - \eta f, \end{cases} \tag{2.1}$$

where $\beta,\sigma,\gamma,D,\xi,\eta,R$ are positive constants, and

$$\chi_{\mathbf{B}(\mathbf{X}_j,R)} := \begin{cases} 1, & \text{if} \quad \mathbf{x}\in\mathbf{B}(\mathbf{X}_j,R); \\ 0, & \qquad \text{otherwise}; \end{cases}$$

with

$$\mathbf{B}(\mathbf{X}_j,R) := \{\mathbf{x} : ||\mathbf{x}-\mathbf{X}_j|| \le R\}.$$

Initial data are given by initial position and velocity for each particle:

$$\mathbf{X}(0)=\mathbf{X}_0,$$
$$\mathbf{V}(0)=\mathbf{V}_0,$$

with $\mathbf{X}=(\mathbf{X}_1,\dots,\mathbf{X}_N)$, $\mathbf{V}=(\mathbf{V}_1,\dots,\mathbf{V}_N)$, and by the initial concentration of signal, that we assume

$$f(\mathbf{x},0) := f_0 = 0. \tag{2.2}$$

We note that equation $(2.1)_3$ can be analytically solved making the classical exponential transformation:

$$f = e^{-\eta t}u,$$

with $u(\mathbf{x},t)$ solution of

$$\partial_t u = D\Delta u + \xi e^{\eta t}\sum_{i=j}^{N}\chi_{\mathbf{B}(\mathbf{X}_j,R)},$$

and $u(\mathbf{x},0)=f_0$. Now, if

$$\Gamma(\mathbf{x},t):=\frac{1}{(4\pi Dt)^{n/2}}e^{-\frac{||\mathbf{x}||^2}{4Dt}}$$

is the fundamental solution of the heat equation on $\mathbb{R}^n$, using the Duhamel's principle we have

$$\begin{aligned} f(\mathbf{x},t) &= (\Gamma(\mathbf{x},t)*f_0)e^{-\eta t}+e^{-\eta t}\int_0^t \Gamma(\mathbf{x},t-\tau)*\left(\xi e^{\eta\tau}\sum_{j=1}^{N}\chi_{\mathbf{B}(\mathbf{X}_j(\tau),R)}\right)d\tau \\ &= \xi\sum_{j=1}^{N}\int_0^t e^{-\eta(t-\tau)}\int_{\mathbb{R}^n}\Gamma(\mathbf{x}-\bar{\mathbf{x}},t-\tau)\chi_{\mathbf{B}(\mathbf{X}_j(\tau),R)}\,d\bar{\mathbf{x}}d\tau \qquad (2.3) \end{aligned}$$

where $*$ is the convolution operation in the variable $\mathbf{x}$, and $f_0=0$ for our initial condition (2.2).

In the following, for analytical and numerical simplicity, we will discuss the case of N particles in $\mathbb{R}^2$. First, if $\mathbf{x}=(x_1,x_2)$ and $\bar{\mathbf{x}}=(\bar{x}_1,\bar{x}_2)$, from (2.3) we can write

$$f(x_1,x_2,t)=\xi\sum_{j=1}^{N}\int_0^t\iint_{\mathbf{B}(\mathbf{X}_j(\tau),R)}\frac{e^{-\eta(t-\tau)}e^{-\frac{(x_1-\bar{x}_1)^2+(x_2-\bar{x}_2)^2}{4(t-\tau)D}}}{4\pi(t-\tau)D}\,d\bar{x}_1\,d\bar{x}_2\,d\tau. \qquad (2.4)$$

With a simple change of variables it is easy to see that the integrand in (2.4) is L^1 with respect to τ in $(0,t)$. In fact, if we define

$$\tilde{x}_1=\frac{x_1-\bar{x}_1}{\sqrt{4(t-\tau)D}},\quad \tilde{x}_2=\frac{x_2-\bar{x}_2}{\sqrt{4(t-\tau)D}}, \qquad (2.5)$$

and

$$\mathbf{\Phi}(\tilde{x}_1,\tilde{x}_2):=\left(-\tilde{x}_1\sqrt{4(t-\tau)D}+x_1,-\tilde{x}_2\sqrt{4(t-\tau)D}+x_2\right),$$

we have the Jacobian

$$\det\left[\partial\mathbf{\Phi}/\partial\tilde{\mathbf{x}}\right]=\begin{vmatrix}-\sqrt{4(t-\tau)D} & 0\\ 0 & -\sqrt{4(t-\tau)D}\end{vmatrix}=4(t-\tau)D.$$

In the new variables (2.4) becomes

$$\begin{aligned} f(x_1,x_2,t) &= \xi\sum_{j=1}^{N}\int_0^t\iint_{\tilde{\mathbf{B}}}\frac{e^{-\eta(t-\tau)}e^{-\frac{\tilde{x}_1^2+\tilde{x}_2^2}{4(t-\tau)D}4(t-\tau)D}}{4\pi(t-\tau)D}4(t-\tau)D\,d\tilde{x}_1\,d\tilde{x}_2\,d\tau \\ &= \frac{\xi}{\pi}\sum_{j=1}^{N}\int_0^t e^{-\eta(t-\tau)}\iint_{\tilde{\mathbf{B}}}e^{-(\tilde{x}_1^2+\tilde{x}_2^2)}\,d\tilde{x}_1\,d\tilde{x}_2\,d\tau, \qquad (2.6) \end{aligned}$$

where $\tilde{\mathbf{B}}$ is obtained from $\mathbf{B}$ under transformation (2.5). In (2.6) the integrand is L^1 in $(0,t)$, with respect to τ.

Now, if $\nabla f = (\partial_{x_1} f, \partial_{x_2} f)$ is the chemotactic gradient, and $\mathbf{X}_i = (X_{i1}, X_{i2})$, $\mathbf{V}_i = (V_{i1}, V_{i2})$ are respectively the position and the velocity of the i-th cell, we obtain

$$\partial_{x_1} f(x_1, x_2, t) = \xi \sum_{j=1}^{N} \int_0^t \iint_{\mathbf{B}(\mathbf{X}_j(\tau),R)} \frac{e^{-\eta(t-\tau)} e^{-\frac{(x_1-\bar{x}_1)^2+(x_2-\bar{x}_2)^2}{4(t-\tau)D}}}{4\pi(t-\tau)D}$$

$$\times \left(-\frac{2(x_1-\bar{x}_1)}{4(t-\tau)D}\right) d\bar{x}_1\, d\bar{x}_2\, d\tau$$

$$= -\xi \sum_{j=1}^{N} \int_0^t \frac{e^{-\eta(t-\tau)}}{4\pi(t-\tau)D} \int_{X_{j2}(\tau)-R}^{X_{j2}(\tau)+R} e^{-\frac{(x_2-\bar{x}_2)^2}{4(t-\tau)D}}$$

$$\times \int_{X_{j1}(\tau)-\sqrt{R^2-(\bar{x}_2-X_{j2}(\tau))^2}}^{X_{j1}(\tau)+\sqrt{R^2-(\bar{x}_2-X_{j2}(\tau))^2}} e^{-\frac{(x_1-\bar{x}_1)^2}{4D(t-\tau)}} \frac{2(x_1-\bar{x}_1)}{4(t-\tau)D} d\bar{x}_1\, d\bar{x}_2\, d\tau$$

$$= -\xi \sum_{j=1}^{N} \int_0^t \frac{e^{-\eta(t-\tau)}}{4\pi(t-\tau)D} \int_{X_{j2}(\tau)-R}^{X_{j2}(\tau)+R} e^{-\frac{(x_2-\bar{x}_2)^2}{4(t-\tau)D}}$$

$$\times \left(e^{-\frac{\left(x_1-X_{j1}(\tau)-\sqrt{R^2-\left[\bar{x}_2-X_{j2}(\tau)\right]^2}\right)^2}{4(t-\tau)D}} - e^{-\frac{\left(x_1-X_{j1}(\tau)+\sqrt{R^2-\left[\bar{x}_2-X_{j2}(\tau)\right]^2}\right)^2}{4(t-\tau)D}} \right) d\bar{x}_2\, d\tau$$

$$= -\xi \sum_{j=1}^{N} \int_0^t \frac{e^{-\eta(t-\tau)}}{4\pi(t-\tau)D} \int_{-R}^{+R} e^{-\frac{(x_2-X_{j2}(\tau)-\tilde{x}_2)^2}{4(t-\tau)D}} \left(e^{-\frac{\left(x_1-X_{j1}(\tau)-\sqrt{R^2-\tilde{x}_2^2}\right)^2}{4(t-\tau)D}} \right.$$

$$\left. -e^{-\frac{\left(x_1-X_{j1}(\tau)+\sqrt{R^2-\tilde{x}_2^2}\right)^2}{4(t-\tau)D}} \right) d\tilde{x}_2\, d\tau, \tag{2.7}$$

where in the last step we have used the change of variables

$$\tilde{x}_2 = \bar{x}_2 - X_{j2}(\tau).$$

Similarly we can proceed for $\partial_{x_2} f(x_1, x_2, t)$.

Finally, substituting (2.7) into $(2.1)_1$ we can summarize, for $i = 1, \dots, N$, the following system:

$$
\begin{cases}
\dot{V}_{i1} &= \dfrac{\beta}{N} \displaystyle\sum_{j=1}^{N} \frac{1}{\left(1 + \frac{||\mathbf{X}_i - \mathbf{X}_j||^2}{R^2}\right)^{\sigma}} (V_{j1} - V_{i1}) \\
&-\gamma\xi \displaystyle\int_0^t \frac{e^{-\eta(t-\tau)}}{4\pi(t-\tau)D} \sum_{j=1}^{N} \int_{-R}^{+R} e^{-\frac{(X_{i2}(t)-X_{j2}(\tau)-\tilde{x}_2)^2}{4(t-\tau)D}} \left(e^{-\frac{\left(X_{i1}(t)-X_{j1}(\tau)-\sqrt{R^2-\tilde{x}_2^2}\right)^2}{4(t-\tau)D}} \right. \\
&\left. -e^{-\frac{\left(X_{i1}(t)-X_{j1}(\tau)+\sqrt{R^2-\tilde{x}_2^2}\right)^2}{4(t-\tau)D}} \right) d\tilde{x}_2 \, d\tau, \\
\dot{V}_{i2} &= \dfrac{\beta}{N} \displaystyle\sum_{j=1}^{N} \frac{1}{\left(1 + \frac{||\mathbf{X}_i - \mathbf{X}_j||^2}{R^2}\right)^{\sigma}} (V_{j2} - V_{i2}) \\
&-\gamma\xi \displaystyle\int_0^t \frac{e^{-\eta(t-\tau)}}{4\pi(t-\tau)D} \sum_{j=1}^{N} \int_{-R}^{+R} e^{-\frac{(X_{i1}(t)-X_{j1}(\tau)-\tilde{x}_1)^2}{4(t-\tau)D}} \left(e^{-\frac{\left(X_{i2}(t)-X_{j2}(\tau)-\sqrt{R^2-\tilde{x}_1^2}\right)^2}{4(t-\tau)D}} \right. \\
&\left. -e^{-\frac{\left(X_{i2}(t)-X_{j2}(\tau)+\sqrt{R^2-\tilde{x}_1^2}\right)^2}{4(t-\tau)D}} \right) d\tilde{x}_1 \, d\tau \\
\dot{X}_{i1} &= V_{i1}, \\
\dot{X}_{i2} &= V_{i2}.
\end{cases}
\tag{2.8}
$$

3. LOCAL EXISTENCE AND UNIQUENESS OF THE SOLUTION

In this section, using a fixed point argumentation, we prove for (2.8) the local existence and uniqueness of the solution. In the next section, then, this result will be extended to a global one.

First, let $\mathbf{y} = (\mathbf{V}_1, \dots, \mathbf{V}_N, \mathbf{X}_1, \dots, \mathbf{X}_N)$ the solution vector, and let

$$\mathbf{q} := (\mathbf{q}_1, \mathbf{q}_2),$$

with

$$q_{1,i1} := \frac{\beta}{N}\sum_{j=1}^{N} \frac{1}{\left(1+\frac{\|\mathbf{X}_j-\mathbf{X}_i\|^2}{R^2}\right)^{\sigma}}(V_{j1}-V_{i1}), \tag{3.1}$$

$$q_{1,i2} := \frac{\beta}{N}\sum_{j=1}^{N} \frac{1}{\left(1+\frac{\|\mathbf{X}_j-\mathbf{X}_i\|^2}{R^2}\right)^{\sigma}}(V_{j2}-V_{i2}), \tag{3.2}$$

$$q_{2,i1} := V_{i1}, \tag{3.3}$$

$$q_{2,i2} := V_{i2}. \tag{3.4}$$

and then

$$\mathbf{p} := (\mathbf{p}_1, \mathbf{p}_2),$$

with

$$p_{1,i1} := \sum_{j=1}^{N}\int_{-R}^{+R} e^{-\frac{(X_{i2}(t)-X_{j2}(\tau)-\tilde{x}_2)^2}{4(t-\tau)D}} \left(e^{-\frac{\left(X_{i1}(t)-X_{j1}(\tau)-\sqrt{R^2-\tilde{x}_2^2}\right)^2}{4(t-\tau)D}} - e^{-\frac{\left(X_{i1}(t)-X_{j1}(\tau)+\sqrt{R^2-\tilde{x}_2^2}\right)^2}{4(t-\tau)D}} \right) d\tilde{x}_2, \tag{3.5}$$

$$p_{1,i2} := \sum_{j=1}^{N}\int_{-R}^{+R} e^{-\frac{(X_{i1}(t)-X_{j1}(\tau)-\tilde{x}_1)^2}{4(t-\tau)D}} \left(e^{-\frac{\left(X_{i2}(t)-X_{j2}(\tau)-\sqrt{R^2-\tilde{x}_1^2}\right)^2}{4(t-\tau)D}} - e^{-\frac{\left(X_{i2}(t)-X_{j2}(\tau)+\sqrt{R^2-\tilde{x}_1^2}\right)^2}{4(t-\tau)D}} \right) d\tilde{x}_1, \tag{3.6}$$

$$p_{2,i1} = p_{2,i2} = 0.$$

Finally, if

$$C(t-\tau) := \frac{\gamma\xi e^{-\eta(t-\tau)}}{4\pi(t-\tau)D},$$

system (2.8) can be written as

$$\dot{\mathbf{y}} = \mathbf{q}(\mathbf{y}) + \int_0^t C(t-\tau)\mathbf{p}(t-\tau, \mathbf{y}(t), \mathbf{y}(\tau))\, d\tau.$$

Integrating from 0 to t we have

$$\mathbf{y} = \mathbf{y}_0 + \int_0^t \mathbf{q}(\mathbf{y}(\tau))\, d\tau + \int_0^t \int_0^s C(s-\tau)\mathbf{p}(s-\tau, \mathbf{y}(s), \mathbf{y}(\tau))\, d\tau\, ds,$$

with $\mathbf{y}_0 = \mathbf{y}(0)$. Then, interchanging the order of integration in the second integral, we have

$$\mathbf{y} = \mathbf{y}_0 + \int_0^t \left[\mathbf{q}(\mathbf{y}(\tau)) + \int_\tau^t C(s-\tau)\mathbf{p}(s-\tau, \mathbf{y}(s), \mathbf{y}(\tau))\, ds\right] d\tau, \tag{3.7}$$

or

$$\mathbf{y} = \mathbf{y}_0 + \int_0^t \left[\mathbf{q}(\mathbf{y}(\tau)) + \mathbf{h}(t, \tau, \mathbf{y}(\tau))\right] \, d\tau, \tag{3.8}$$

with

$$\mathbf{h}(t, \tau, \mathbf{y}(\tau)) := \int_\tau^t C(s-\tau)\mathbf{p}(s-\tau, \mathbf{y}(s), \mathbf{y}(\tau)) \, ds.$$

For a discussion of such type of equations see, for example, Burton (2005), Khalil (2002), and also Wazwaz (2011), Lakshmikantham and Rama (1995).

Now, let $a, b > 0$. We consider the set

$$S = \left\{(t, \tau, s, \mathbf{y}) : 0 \leq \tau \leq s \leq t \leq a, \, \|\mathbf{y}(t) - \mathbf{y}_0\| \leq b\right\}.$$

Since $\mathbf{q}(\mathbf{y})$ is continuous on S, we can define

$$M_1 = \max_S \|\mathbf{q}(\mathbf{y})\|. \tag{3.9}$$

Then, to prove that $\mathbf{h}(t, \tau, \mathbf{y}(\tau))$ is continuous in S, firstly we prove that $C(s-\tau)\mathbf{p}(s-\tau, \mathbf{y}(s), \mathbf{y}(\tau))$ in $L^1(\tau, t)$ with respect to variable s. It is enough to demonstrate the integrability around $s = \tau$. Starting from (3.5), we consider $p_{1,i1}(s-\tau, \mathbf{y}(s), \mathbf{y}(\tau))$, and the change of variables

$$\frac{X_{i2} - X_{j2} - \tilde{x}_2}{\sqrt{4(s-\tau)D}} = z. \tag{3.10}$$

Since the quantity in brackets is bounded by 1, we have

$$\begin{aligned}
|p_{1,i1}(s-\tau, \mathbf{y}(s), \mathbf{y}(\tau))| &\leq \sum_{j=1}^N \int_{-R}^{+R} e^{-\frac{(X_{i2}(s) - X_{j2}(\tau) - \tilde{x}_2)^2}{4(s-\tau)D}} \, d\tilde{x}_2 \\
&= \sqrt{4(s-\tau)D} \sum_{j=1}^N \int_{\frac{X_{i2} - X_{j2} - R}{\sqrt{4(s-\tau)D}}}^{\frac{X_{i2} - X_{j2} + R}{\sqrt{4(s-\tau)D}}} e^{-z^2} \, dz \\
&\leq \sqrt{4(s-\tau)D} \sum_{j=1}^N \int_{-\infty}^{+\infty} e^{-z^2} \, dz \\
&= \bar{M}\sqrt{4(s-\tau)D},
\end{aligned}$$

with

$$\bar{M} := N \int_{-\infty}^{+\infty} e^{-z^2} \, dz. \tag{3.11}$$

The same holds for $p_{1,i2}$ in (3.6), so we can write

$$\|\mathbf{p}(s-\tau, \mathbf{y}(s), \mathbf{y}(\tau))\| \leq \bar{M}\sqrt{2N}\sqrt{4(s-\tau)D}, \tag{3.12}$$

and

$$|C(s-\tau)| \, \|\mathbf{p}(s-\tau, \mathbf{y}(s), \mathbf{y}(\tau))\| \leq \frac{\gamma\xi\bar{M}\sqrt{2N}e^{-\eta(s-\tau)}}{2\pi\sqrt{(s-\tau)D}}. \tag{3.13}$$

Now $C(s-\tau)\mathbf{p}(s-\tau,\mathbf{y}(s),\mathbf{y}(\tau))$ is continuous in $\mathbf{y}$ and, from (3.13), it is $L^1(\tau,t)$ with respect to variable s, so $\mathbf{h}(t,\tau,\mathbf{y}(\tau))$ is continuous in S, and we can define

$$M_2 = \max_S \|\mathbf{h}(t,\tau,\mathbf{y}(\tau))\| \,. \tag{3.14}$$

To prove local existence and uniqueness, we want to obtain a Lipschitz condition in S for the functions $\mathbf{q}$ and $\mathbf{p}$ with respect to the variable $\mathbf{y}$. First, because of $\mathbf{q}$ is C^1 on S, the Jacobian matrix $[\partial\mathbf{q}/\partial\mathbf{y}]$ is bounded on S uniformly in τ, so $\mathbf{q}$ satisfies the Lipschitz condition

$$\|\mathbf{q}(\mathbf{y}_1) - \mathbf{q}(\mathbf{y}_2)\| \le L_1 \|\mathbf{y}_1 - \mathbf{y}_2\| \,, \tag{3.15}$$

with L_1 positive constant and $(t,\tau,s,\mathbf{y}_1)$, $(t,\tau,s,\mathbf{y}_2) \in S$.

Then, from (3.5) we define

$$\bar{p}_{1,i1,j1}(s-\tau,\mathbf{y}(s),\mathbf{y}(\tau),\tilde{x}_2) := e^{-\frac{\left(X_{i1}(s)-X_{j1}(\tau)-\sqrt{R^2-\tilde{x}_2^2}\right)^2}{4(s-\tau)D}} - e^{-\frac{\left(X_{i1}(s)-X_{j1}(\tau)+\sqrt{R^2-\tilde{x}_2^2}\right)^2}{4(s-\tau)D}} . \tag{3.16}$$

For the Jacobian matrix of (3.16), hold the following equalities

$$\begin{aligned}
\frac{\partial \bar{p}_{1,i1,j1}}{\partial V_{k1}} &= \frac{\partial \bar{p}_{1,i1,j1}}{\partial V_{k2}} = 0 \\
\frac{\partial \bar{p}_{1,i1,j1}}{\partial X_{k1}} &= \begin{cases}
-\left[e^{-\frac{\left(X_{i1}(s)-X_{j1}(\tau)-\sqrt{R^2-\tilde{x}_2^2}\right)^2}{4(s-\tau)D}} \frac{X_{i1}(s)-X_{j1}(\tau)-\sqrt{R^2-\tilde{x}_2^2}}{2(s-\tau)D} \right. \\
\qquad \left. -e^{-\frac{\left(X_{i1}(s)-X_{j1}(\tau)+\sqrt{R^2-\tilde{x}_2^2}\right)^2}{4(s-\tau)D}} \frac{X_{i1}(s)-X_{j1}(\tau)+\sqrt{R^2-\tilde{x}_2^2}}{2(s-\tau)D} \right], & k = i; \\
\delta_{jk} \left[e^{-\frac{\left(X_{i1}(s)-X_{j1}(\tau)-\sqrt{R^2-\tilde{x}_2^2}\right)^2}{4(s-\tau)D}} \frac{X_{i1}(s)-X_{j1}(\tau)-\sqrt{R^2-\tilde{x}_2^2}}{2(s-\tau)D} \right. \\
\qquad \left. -e^{-\frac{\left(X_{i1}(s)-X_{j1}(\tau)+\sqrt{R^2-\tilde{x}_2^2}\right)^2}{4(s-\tau)D}} \frac{X_{i1}(s)-X_{j1}(\tau)+\sqrt{R^2-\tilde{x}_2^2}}{2(s-\tau)D} \right], & k \neq i;
\end{cases} \\
\frac{\partial \bar{p}_{1,i1,j1}}{\partial X_{k2}} &= 0.
\end{aligned}$$

Since these quantities are bounded in S uniformly in $\tilde{x}_2$, τ, s, we can write

$$\begin{aligned}
&|\bar{p}_{1,i1,j1}(s-\tau,\mathbf{y}_1(s),\mathbf{y}_1(\tau),\tilde{x}_2) - \bar{p}_{1,i1,j1}(s-\tau,\mathbf{y}_2(s),\mathbf{y}_2(\tau),\tilde{x}_2)| \\
&\le l_2 \left(\|\mathbf{y}_1(s) - \mathbf{y}_2(s)\| + \|\mathbf{y}_1(\tau) - \mathbf{y}_2(\tau)\|\right),
\end{aligned} \tag{3.17}$$

where l_2 is a positive constant, and $(\tau, s, \mathbf{y}_1)$, $(\tau, s, \mathbf{y}_2) \in S$. From this we deduce

$$\begin{aligned}
&|p_{1,i1}(s-\tau, \mathbf{y}_1(s), \mathbf{y}_1(\tau)) - p_{1,i1}(s-\tau, \mathbf{y}_2(s), \mathbf{y}_2(\tau))| \\
&\le \sum_{j=1}^{N} \int_{-R}^{+R} \left| e^{-\frac{(X_{i2}^{(1)}(s) - X_{j2}^{(1)}(\tau) - \tilde{x}_2)^2}{4D(s-\tau)}} - e^{-\frac{(X_{i2}^{(2)}(s) - X_{j2}^{(2)}(\tau) - \tilde{x}_2)^2}{4D(s-\tau)}} \right| \\
&\times |\bar{p}_{1,i1,j1}(s-\tau, \mathbf{y}_1(s), \mathbf{y}_1(\tau), \tilde{x}_2) - \bar{p}_{1,i1,j1}(s-\tau, \mathbf{y}_2(s), \mathbf{y}_2(\tau), \tilde{x}_2)| \, d\tilde{x}_2 \\
&=_{(3.17),(3.10)} \sqrt{4D(s-\tau)} l_2 \left(\|\mathbf{y}_1(s) - \mathbf{y}_2(s)\| + \|\mathbf{y}_1(\tau) - \mathbf{y}_2(\tau)\| \right) \\
&\times \sum_{j=1}^{N} \left(\int_{\frac{X_{i2}^{(1)}(s) - X_{j2}^{(1)}(\tau) - R}{\sqrt{4(s-\tau)D}}}^{\frac{X_{i2}^{(1)}(s) - X_{j2}^{(1)}(\tau) + R}{\sqrt{4(s-\tau)D}}} e^{-z^2} \, dz + \int_{\frac{X_{i2}^{(2)}(s) - X_{j2}^{(2)}(\tau) - R}{\sqrt{4(s-\tau)D}}}^{\frac{X_{i2}^{(2)}(s) - X_{j2}^{(2)}(\tau) + R}{\sqrt{4(s-\tau)D}}} e^{-z^2} \, dz \right) \\
&\le \sqrt{4D(s-\tau)} l_2 \left(\|\mathbf{y}_1(s) - \mathbf{y}_2(s)\| + \|\mathbf{y}_1(\tau) - \mathbf{y}_2(\tau)\| \right) 2 \sum_{j=1}^{N} \int_{-\infty}^{+\infty} e^{-z^2} \, dz \\
&=_{(3.11)} \sqrt{4D(s-\tau)} 2\bar{M} l_2 \left(\|\mathbf{y}_1(s) - \mathbf{y}_2(s)\| + \|\mathbf{y}_1(\tau) - \mathbf{y}_2(\tau)\| \right),
\end{aligned}$$

where we have used the change of variables (3.10). Moreover, $X^{(1)}$, $X^{(2)}$ are the variables belonging respectively to the vectors $\mathbf{y}_1$, $\mathbf{y}_2$, and $(t, \tau, s, \mathbf{y}_1)$, $(t, \tau, s, \mathbf{y}_2) \in S$.

The same can be done for $p_{1,i2}$, so $\mathbf{p}$ satisfy the following condition in $\mathbf{y}$ on S:

$$\begin{aligned}
\|\mathbf{p}(s-\tau, \mathbf{y}_1(s), \mathbf{y}_1(\tau)) - \mathbf{p}(s-\tau, \mathbf{y}_2(s), \mathbf{y}_2(\tau))\| \le \sqrt{4D(s-\tau)} L_2 \left(\|\mathbf{y}_1(s) - \mathbf{y}_2(s)\| \right. \\
\left. + \|\mathbf{y}_1(\tau) - \mathbf{y}_2(\tau)\| \right), \qquad (3.18)
\end{aligned}$$

with L_2 a suitable positive constant that incorporates previous constants, and $(\tau, s, \mathbf{y}_1)$, $(\tau, s, \mathbf{y}_2) \in S$.

Now, we fix

$$T = \min \left[a, \frac{b}{M_1 + M_2}, \frac{1}{L_1 + 2L_2 M} \right], \qquad (3.19)$$

with M_1, M_2 given by (3.9)–(3.14), and

$$M := \int_0^{+\infty} |C(z)| \sqrt{4Dz} \, dz. \qquad (3.20)$$

Then we prove the following

Theorem 1. *Equation* (3.8) *has a unique solution on* $[0, T]$*, where* T *is defined in* (3.19).

Proof. We consider the functional space

$$\mathcal{B} = \left\{ \mathbf{y} \in C^0([0, T]) : ||\mathbf{y} - \mathbf{y}_0||_{C^0} \le b \right\},$$

where

$$||\mathbf{y} - \mathbf{z}||_{C^0} := \sup_{0 \le t \le T} \|\mathbf{y}(t) - \mathbf{z}(t)\|,$$

and we define the functional $\mathbf{A} : \mathcal{B} \to \mathcal{B}$ as

$$\mathbf{A}(\mathbf{y})(t) := \mathbf{y}_0 + \int_0^t \left[\mathbf{q}(\mathbf{y}(\tau)) + \mathbf{h}(t, \tau, \mathbf{y}(\tau)) \right] d\tau,$$

To see that $\mathbf{A} : \mathcal{B} \to \mathcal{B}$ notice that $\mathbf{y}$ continuous implies $\mathbf{A}(\mathbf{y})$ continuous, because $\mathbf{q}$ and $\mathbf{h}$ are continuous, and that

$$\begin{aligned}
\|\mathbf{A}(\mathbf{y}) - \mathbf{y}_0\|_{C^0} &= \sup_{0\le t\le T} \|\mathbf{A}(\mathbf{y})(t) - \mathbf{y}_0\| \\
&\le \sup_{0\le t\le T} \int_0^t \left(\|\mathbf{q}(\mathbf{y}(\tau))\| + \|\mathbf{h}(t,\tau,\mathbf{y}(\tau))\|\right) d\tau \\
&\le (M_1 + M_2)T \\
&\le b,
\end{aligned}$$

where we have used (3.9), (3.14) and, in the last inequality, (3.19). To see that $\mathbf{A}$ is a contraction mapping, notice that if $\mathbf{y}_1$ and $\mathbf{y}_2 \in \mathcal{B}$ then

$$\begin{aligned}
\|\mathbf{A}(\mathbf{y}_1) - \mathbf{A}(\mathbf{y}_2)\|_{C^0} &= \sup_{0\le t\le T} \|\mathbf{A}(\mathbf{y}_1)(t) - \mathbf{A}(\mathbf{y}_2)(t)\| \\
&\le \sup_{0\le t\le T} \int_0^t (\|\mathbf{q}(\mathbf{y}_1(\tau)) - \mathbf{q}(\mathbf{y}_2(\tau))\| \\
&+ \int_\tau^t |C(s-\tau)| \, \|\mathbf{p}(s-\tau,\mathbf{y}_1(s),\mathbf{y}_1(\tau)) - \mathbf{p}(s-\tau,\mathbf{y}_2(s),\mathbf{y}_2(\tau))\|) \, ds \, d\tau \\
&\le_{(3.15),(3.18)} \sup_{0\le t\le T} \int_0^t [L_1 \|\mathbf{y}_1(\tau) - \mathbf{y}_2(\tau)\| + L_2 \int_\tau^t |C(s-\tau)| \sqrt{4D(s-\tau)} \\
&\times (\|\mathbf{y}_1(s) - \mathbf{y}_2(s)\| + \|\mathbf{y}_1(\tau) - \mathbf{y}_2(\tau)\|)] \, ds \, d\tau \\
&\le L_1 T \|\mathbf{y}_1 - \mathbf{y}_2\|_{C^0} + 2L_2 \|\mathbf{y}_1 - \mathbf{y}_2\|_{C^0} \\
&\times \sup_{0\le t\le T} \int_0^t \int_\tau^t |C(s-\tau)| \sqrt{4D(s-\tau)} \, ds \, d\tau \\
&= \left(L_1 T + 2L_2 \sup_{0\le t\le T} \int_0^t \int_0^{t-\tau} |C(z)| \sqrt{4Dz} \, dz \, d\tau \right) \|\mathbf{y}_1 - \mathbf{y}_2\|_{C^0} \\
&\le \left(L_1 T + 2L_2 \int_0^T \int_0^{+\infty} |C(z)| \sqrt{4Dz} \, dz \, d\tau \right) \|\mathbf{y}_1 - \mathbf{y}_2\|_{C^0} \\
&= (L_1 + 2L_2 M) T \|\mathbf{y}_1 - \mathbf{y}_2\|_{C^0} .
\end{aligned}$$

From (3.19) the constant $(L_1 + 2L_2 M)T \in (0,1)$. The Banach-Caccioppoli fixed-point theorem completes the proof.

4. Global existence and uniqueness of the solution

To obtain global existence and uniqueness for (3.7) we will use a principle of continuation of solutions. We will prove that bounded solutions can be continued to $t = +\infty$. The following general result, adapted for equation (3.7), provides a condition for the continuation of solutions.

Proposition 1. *Let* $\mathbf{y}(t)$ *be a solution of* (3.7) *on a interval* $[0,T)$, *if there is a constant* P *with* $\|\mathbf{y} - \mathbf{y}_0\| \le P$ *on* $[0,T)$, *then there is a* $\bar{T} > T$ *such that* $\mathbf{y}(t)$ *can be continued to* $[0,\bar{T}]$.

Proof. We show that $\lim_{t\to T^-} \mathbf{y}(t)$ exists, so we can applied Theorem 1 starting at $t = T$, and this completes the proof.

Let t_n be a monotonic increasing sequence with limit T, and let

$$\bar{U} = \{(t, \tau, s, \mathbf{y}) : 0 \leq \tau \leq s \leq t \leq T,\ \|\mathbf{y} - \mathbf{y}_0\| \leq P\}.$$

We prove that $\{\mathbf{y}(t_n)\}$ is a Cauchy sequence. If $t_m > t_n$, from (3.7) we have

$$\begin{aligned}
\|\mathbf{y}(t_m) - \mathbf{y}(t_n)\| &= \left\| \int_0^{t_m} \left[\mathbf{q}(\mathbf{y}(\tau)) + \int_\tau^{t_m} C(s-\tau)\mathbf{p}(s-\tau, \mathbf{y}(s), \mathbf{y}(\tau))\, ds \right] d\tau \right. \\
&\quad \left. - \int_0^{t_n} \left[\mathbf{q}(\mathbf{y}(\tau)) + \int_\tau^{t_n} C(s-\tau)\mathbf{p}(s-\tau, \mathbf{y}(s), \mathbf{y}(\tau))\, ds \right] d\tau \right\| \\
&\leq \int_0^{t_n} \left\| \int_\tau^{t_m} C(s-\tau)\mathbf{p}(s-\tau, \mathbf{y}(s), \mathbf{y}(\tau))\, ds \right. \\
&\quad \left. - \int_\tau^{t_n} C(s-\tau)\mathbf{p}(s-\tau, \mathbf{y}(s), \mathbf{y}(\tau))\, ds \right\| d\tau \\
&\quad + \left\| \int_{t_n}^{t_m} \left[\mathbf{q}(\mathbf{y}(\tau)) + \int_\tau^{t_m} C(s-\tau)\mathbf{p}(s-\tau, \mathbf{y}(s), \mathbf{y}(\tau))\, ds \right] d\tau \right\| \\
&\leq \int_0^{t_n} \left\| \int_{t_n}^{t_m} C(s-\tau)\mathbf{p}(s-\tau, \mathbf{y}(s), \mathbf{y}(\tau))\, ds \right\| d\tau \\
&\quad + \left\| \int_{t_n}^{t_m} \int_\tau^{t_m} C(s-\tau)\mathbf{p}(s-\tau, \mathbf{y}(s), \mathbf{y}(\tau))\, ds\, d\tau \right\| \\
&\quad + \left\| \int_{t_n}^{t_m} \mathbf{q}(\mathbf{y}(\tau))\, d\tau \right\| \\
&\leq \int_0^{t_n} \int_{t_n}^{t_m} \|C(s-\tau)\mathbf{p}(s-\tau, \mathbf{y}(s), \mathbf{y}(\tau))\|\, ds\, d\tau \\
&\quad + \int_{t_n}^{t_m} \int_\tau^{t_m} \|C(s-\tau)\mathbf{p}(s-\tau, \mathbf{y}(s), \mathbf{y}(\tau))\|\, ds\, d\tau \\
&\quad + \int_{t_n}^{t_m} \|\mathbf{q}(\mathbf{y}(\tau))\|\, d\tau.
\end{aligned}$$

In the last inequality the third integral tends to zero as $n, m \to +\infty$, because $\mathbf{q}$ is bounded on $\bar{U}$ and $t_m, t_n \to T$. Also the first two integrals go to zero as $n, m \to +\infty$, because of (3.13). The proof is completed.

Now, from Proposition 1, we obtain the following

Theorem 2. *Equation* (3.8) *has a unique global solution for all* $t \geq 0$.

Proof. First, equations (3.1)–(3.4) imply

$$\begin{aligned}
|q_{1,i1}| \leq 2\beta||\mathbf{y}||, \quad |q_{1,i2}| \leq 2\beta||\mathbf{y}||, \\
|q_{2,i1}| \leq ||\mathbf{y}||, \quad |q_{2,i2}| \leq ||\mathbf{y}||,
\end{aligned}$$

so that

$$||\mathbf{q}|| \leq \sqrt{2N(4\beta^2 + 1)}||\mathbf{y}||.$$

Then (3.12) establishes

$$\|\mathbf{p}(s-\tau,\mathbf{y}(s),\mathbf{y}(\tau))\| \leq \bar{M}\sqrt{2N}\sqrt{4D(s-\tau)},$$

so from (3.7) we have

$$\begin{aligned} ||\mathbf{y}|| &\leq ||\mathbf{y}_0|| + \sqrt{2N(4\beta^2+1)}\int_0^t ||\mathbf{y}(\tau)||\,d\tau \\ &+ \bar{M}\sqrt{2N}\int_0^t\int_\tau^t |C(s-\tau)|\,\sqrt{4D(s-\tau)}\,ds\,d\tau \\ &= ||\mathbf{y}_0|| + \sqrt{2N(4\beta^2+1)}\int_0^t ||\mathbf{y}(\tau)||\,d\tau + \bar{M}\sqrt{2N}\int_0^t\int_0^{t-\tau} |C(z)|\,\sqrt{4Dz}\,dz\,d\tau \\ &\leq ||\mathbf{y}_0|| + \sqrt{2N(4\beta^2+1)}\int_0^t ||\mathbf{y}(\tau)||\,d\tau + \bar{M}\sqrt{2N}\int_0^t\int_0^{+\infty} |C(z)|\,\sqrt{4Dz}\,dz\,d\tau \\ &= ||\mathbf{y}_0|| + \sqrt{2N(4\beta^2+1)}\int_0^t ||\mathbf{y}(\tau)||\,d\tau + M\bar{M}\sqrt{2N}t, \end{aligned}$$

where we have set $z = s-\tau$, and M is given by (3.20).

Now, for each $0 \leq t < T$,

$$||\mathbf{y}|| \leq \left(||\mathbf{y}_0|| + M\bar{M}\sqrt{2N}T\right) + \sqrt{2N(4\beta^2+1)}\int_0^t ||\mathbf{y}(\tau)||\,d\tau,$$

so that

$$||\mathbf{y}|| \leq \left(||\mathbf{y}_0|| + M\bar{M}\sqrt{2N}T\right)e^{t\sqrt{2N(4\beta^2+1)}}$$

by the Gronwall's inequality. Since solution remains bounded, for Proposition 1, it can be continued to all $[0,+\infty)$.

5. ASYMPTOTIC PROPERTIES ON THE LINEARIZED SYSTEM

In this section we prove some asymptotic properties on the linearized form of system (2.8), that for convenience we recall here:

$$
\begin{cases}
\begin{aligned}
\dot{V}_{i1} &= \frac{\beta}{N}\sum_{j=1}^{N}\frac{1}{\left(1+\frac{||\mathbf{X}_i-\mathbf{X}_j||^2}{R^2}\right)^{\sigma}}(V_{j1}-V_{i1}) \\
&\quad -\int_0^t C(t-\tau)\sum_{j=1}^{N}\int_{-R}^{+R} e^{-\frac{(X_{i2}(t)-X_{j2}(\tau)-\tilde{x}_2)^2}{4(t-\tau)D}}\left(e^{-\frac{\left(X_{i1}(t)-X_{j1}(\tau)-\sqrt{R^2-\tilde{x}_2^2}\right)^2}{4(t-\tau)D}}\right. \\
&\quad \left. -e^{-\frac{\left(X_{i1}(t)-X_{j1}(\tau)+\sqrt{R^2-\tilde{x}_2^2}\right)^2}{4(t-\tau)D}}\right) d\tilde{x}_2\, d\tau, \\
\dot{V}_{i2} &= \frac{\beta}{N}\sum_{j=1}^{N}\frac{1}{\left(1+\frac{||\mathbf{X}_i-\mathbf{X}_j||^2}{R^2}\right)^{\sigma}}(V_{j2}-V_{i2}) \\
&\quad -\int_0^t C(t-\tau)\sum_{j=1}^{N}\int_{-R}^{+R} e^{-\frac{(X_{i1}(t)-X_{j1}(\tau)-\tilde{x}_1)^2}{4(t-\tau)D}}\left(e^{-\frac{\left(X_{i2}(t)-X_{j2}(\tau)-\sqrt{R^2-\tilde{x}_1^2}\right)^2}{4(t-\tau)D}}\right. \\
&\quad \left. -e^{-\frac{\left(X_{i2}(t)-X_{j2}(\tau)+\sqrt{R^2-\tilde{x}_1^2}\right)^2}{4(t-\tau)D}}\right) d\tilde{x}_1\, d\tau, \\
\dot{X}_{i1} &= V_{i1}, \\
\dot{X}_{i2} &= V_{i2},
\end{aligned}
\end{cases}
\tag{5.1}
$$

with

$$
C(t-\tau) := \frac{\gamma\xi e^{-\eta(t-\tau)}}{4\pi(t-\tau)D}. \tag{5.2}
$$

We are interested in the equilibrium points that satisfy the condition:

$$
\begin{cases}
\mathbf{X}_i(t) = \mathbf{X}_{\text{eq}}(t), & \forall i, \quad \forall t; \\
\mathbf{V}_i(t) = \mathbf{0}, & \forall i;
\end{cases}
\quad \Leftrightarrow \quad \mathbf{X}_i(t) = \mathbf{X}_{\text{eq}} = \text{constant}, \quad \forall i. \tag{5.3}
$$

Equation (5.3) means that all particles are in a same position for all times. Now, to make a first-order approximation of (2.8), we consider the following Taylor expansions around points

(5.3):

$$\begin{aligned}
F_1\left(\mathbf{X}_j - \mathbf{X}_i, V_{j1} - V_{i1}\right) :=& \frac{1}{\left(1 + \frac{\|\mathbf{X}_j - \mathbf{X}_i\|^2}{R^2}\right)^{\sigma}} (V_{j1} - V_{i1}) && (5.4)\\
=& \, V_{j1} - V_{1i} + \rho_1(\mathbf{X}_j - \mathbf{X}_i, V_{j1} - V_{i1}), && (5.5)\\
F_2\left(t-\tau, X_{i2}(t) - X_{j2}(\tau), \tilde{x}_2\right) :=& e^{-\frac{(X_{i2}(t) - X_{j2}(\tau) - \tilde{x}_2)^2}{4(t-\tau)D}} && (5.6)\\
=& e^{-\frac{\tilde{x}_2^2}{4(t-\tau)D}} + \rho_2(t-\tau, X_{i2}(t) - X_{j2}(\tau), \tilde{x}_2), && (5.7)\\
F_3\left(t-\tau, X_{i1}(t) - X_{j1}(\tau), \tilde{x}_2\right) :=& e^{-\frac{\left(X_{i1}(t) - X_{j1}(\tau) \pm \sqrt{R^2 - \tilde{x}_2^2}\right)^2}{4(t-\tau)D}} && (5.8)\\
=& e^{-\frac{R^2 - \tilde{x}_2^2}{4(t-\tau)D}} \mp e^{-\frac{R^2 - \tilde{x}_2^2}{4(t-\tau)D}} \frac{\sqrt{R^2 - \tilde{x}_2^2}}{2(t-\tau)D} \left(X_{i1}(t) - X_{j1}(\tau)\right)\\
&+ \rho_3(t-\tau, X_{i1}(t) - X_{j1}(\tau), \tilde{x}_2), && (5.9)
\end{aligned}$$

where the functions ρ_1 and ρ_3 contain the nonlinear terms, while ρ_2 contains the linear and the nonlinear terms. Similarly we can treat equation $(5.1)_2$.

From (5.4)–(5.9), we linearize equation $(5.1)_1$ in the form

$$\begin{aligned}
\dot{V_{i1}} =& \frac{\beta}{N} \sum_{j=1}^{N} (V_{j1}(t) - V_{i1}(t)) - \int_0^t \frac{C(t-\tau)}{2(t-\tau)D} \int_{-R}^{+R} e^{-\frac{\tilde{x}_2^2}{4(t-\tau)D}} e^{-\frac{R^2 - \tilde{x}_2^2}{4(t-\tau)D}} \sqrt{R^2 - \tilde{x}_2}\\
&\times \sum_{j=1}^{N} \left(X_{i1}(t) - X_{j1}(\tau) + X_{i1}(t) - X_{j1}(\tau)\right) d\tilde{x}_2 \, d\tau\\
=& \frac{\beta}{N} \sum_{j=1}^{N} (V_{j1}(t) - V_{i1}(t)) - \int_0^t \frac{C(t-\tau) e^{-\frac{R^2}{4(t-\tau)D}}}{(t-\tau)D} \int_{-R}^{+R} \sqrt{R^2 - \tilde{x}_2^2} \, d\tilde{x}_2\\
&\times \sum_{j=1}^{N} \left(X_{i1}(t) - X_{j1}(\tau)\right) d\tau\\
=& \frac{\beta}{N} \sum_{j=1}^{N} (V_{j1}(t) - V_{i1}(t)) - \int_0^t \bar{C}(t-\tau) \sum_{j=1}^{N} \left(X_{i1}(t) - X_{j1}(\tau)\right) d\tau,
\end{aligned}$$

with

$$\bar{C}(t-\tau) := \frac{\pi R^2 C(t-\tau) e^{-\frac{R^2}{4(t-\tau)D}}}{2(t-\tau)D}. \tag{5.10}$$

Similarly it can be done for $\dot{V}_{i2}$. Finally, we obtain

$$\begin{cases} \dot{V}_{i1} &= \dfrac{\beta}{N}\displaystyle\sum_{j=1}^{N}(V_{j1}(t)-V_{i1}(t)) - \int_0^t \bar{C}(t-\tau)\sum_{j=1}^{N}\left(X_{i1}(t)-X_{j1}(\tau)\right)\,d\tau, \\ \dot{V}_{i2} &= \dfrac{\beta}{N}\displaystyle\sum_{j=1}^{N}(V_{j2}(t)-V_{i2}(t)) - \int_0^t \bar{C}(t-\tau)\sum_{j=1}^{N}\left(X_{i2}(t)-X_{j2}(\tau)\right)\,d\tau, \\ \dot{X}_{i1} &= V_{i1}, \\ \dot{X}_{i2} &= V_{i2}. \end{cases} \tag{5.11}$$

First, we are interested to establish a time-asymptotic convergence property of all particles towards a same position and a same velocity. For this it is convenient to introduce the centre of mass system, in which equations (5.11) become a nonautonomous system of ordinary differential equation, decoupled with respect to the i-th particle and with respect to the two components of each position and velocity vector. Then the equation of the centre of mass can be studied apart.

We define position and velocity of the centre of mass of a system of N particles with same mass, as

$$\mathbf{X}_{\mathrm{CM}} := \frac{1}{N}\sum_{i=1}^{N}\mathbf{X}_i, \tag{5.12}$$

$$\mathbf{V}_{\mathrm{CM}} := \frac{1}{N}\sum_{i=1}^{N}\mathbf{V}_i, \tag{5.13}$$

and we consider the new variables

$$\bar{\mathbf{X}}_i := \mathbf{X}_i - \mathbf{X}_{\mathrm{CM}}, \tag{5.14}$$

$$\bar{\mathbf{V}}_i := \mathbf{V}_i - \mathbf{V}_{\mathrm{CM}}. \tag{5.15}$$

In variables (5.14)–(5.15) the equilibrium condition (5.3) becomes

$$(\bar{\mathbf{X}}_i, \bar{\mathbf{V}}_i) = (\mathbf{0}, \mathbf{0}), \quad \forall i = 1, \dots, N, \tag{5.16}$$

moreover the following identities hold:

$$\sum_{i=1}^{N}\bar{\mathbf{X}}_i = \mathbf{0}, \tag{5.17}$$

$$\sum_{i=1}^{N}\bar{\mathbf{V}}_i = \mathbf{0}. \tag{5.18}$$

If $\mathbf{V}_{\mathrm{CM}} = (V_{\mathrm{CM}1}, V_{\mathrm{CM}2})$ and $\mathbf{X}_{\mathrm{CM}} = (X_{\mathrm{CM}1}, X_{\mathrm{CM}2})$, from (5.11) we have

$$\begin{aligned}
\dot{V}_{\mathrm{CM}1} &= \frac{1}{N}\sum_{i=1}^{N}\dot{V}_{i1} = \frac{1}{N}\frac{\beta}{N}\sum_{i=1}^{N}\sum_{j=1}^{N}(V_{j1}(t) - V_{i1}(t)) \\
&- \frac{1}{N}\int_0^t \bar{C}(t-\tau)\sum_{i=1}^{N}\sum_{j=1}^{N}\left(X_{i1}(t) - X_{j1}(\tau)\right)\,d\tau \\
&= \frac{1}{N}\frac{\beta}{N}\sum_{i=1}^{N}(NV_{\mathrm{CM}1}(t) - NV_{i1}(t)) \\
&- \frac{1}{N}\int_0^t \bar{C}(t-\tau)\sum_{i=1}^{N}\left(NX_{i1}(t) - NX_{\mathrm{CM}1}(\tau)\right)\,d\tau \\
&= \frac{1}{N}\frac{\beta}{N}(N^2V_{\mathrm{CM}1}(t) - N^2V_{\mathrm{CM}1}(t)) \\
&- \frac{1}{N}\int_0^t \bar{C}(t-\tau)\left(N^2X_{\mathrm{CM}1}(t) - N^2X_{\mathrm{CM}1}(\tau)\right)\,d\tau \\
&= -\int_0^t \bar{C}(t-\tau)\left(NX_{\mathrm{CM}1}(t) - NX_{\mathrm{CM}1}(\tau)\right)\,d\tau, \qquad (5.19)
\end{aligned}$$

where we have used definitions (5.12)–(5.13). The same holds for $\dot{V}_{\mathrm{CM}2}$:

$$\dot{V}_{\mathrm{CM}2} = -\int_0^t \bar{C}(t-\tau)\left(NX_{\mathrm{CM}2}(t) - NX_{\mathrm{CM}2}(\tau)\right)\,d\tau. \qquad (5.20)$$

In the variables $(\bar{\mathbf{X}}_i, \bar{\mathbf{V}}_i)$, taking into account (5.19)–(5.20), equations $(5.11)_{1,3}$ become

$$\begin{aligned}
\dot{\bar{V}}_{i1} &= -\dot{V}_{\mathrm{CM}1} + \frac{\beta}{N}\sum_{j=1}^{N}(\bar{V}_{j1}(t) - \bar{V}_{i1}(t)) \\
&- \int_0^t \bar{C}(t-\tau)\sum_{j=1}^{N}\left(\bar{X}_{i1}(t) - \bar{X}_{j1}(\tau) + X_{\mathrm{CM}1}(t) - X_{\mathrm{CM}1}(\tau)\right)\,d\tau \\
&= \frac{\beta}{N}\left(\sum_{j=1}^{N}\bar{V}_{j1}(t) - \sum_{j=1}^{N}\bar{V}_{i1}(t)\right) \\
&- \int_0^t \bar{C}(t-\tau)(N\bar{X}_{i1}(t) - \sum_{j=1}^{N}\bar{X}_{j1}(\tau) + NX_{\mathrm{CM}1}(t) - NX_{\mathrm{CM}1}(\tau) \\
&- NX_{\mathrm{CM}1}(t) + NX_{\mathrm{CM}1}(\tau))\,d\tau \\
&= -\beta\bar{V}_{i1}(t) - N\left(\int_0^t \bar{C}(t-\tau)\,d\tau\right)\bar{X}_{i1}(t),
\end{aligned}$$

where we have used (5.17)–(5.18), and

$$\dot{\bar{X}}_{i1} = -\dot{X}_{\mathrm{CM}1} + \bar{V}_{i1} + V_{\mathrm{CM}1} = \bar{V}_{i1}.$$

Similarly for $\dot{\bar{V}}_{i2}$ and $\dot{\bar{X}}_{i2}$.

Finally, we can write the following system:

$$\begin{cases} \dot{\bar{V}}_{i1} = -\beta \bar{V}_{i1}(t) - g(t)\bar{X}_{i1}(t), \\ \dot{\bar{V}}_{i2} = -\beta \bar{V}_{i2}(t) - g(t)\bar{X}_{i2}(t), \\ \dot{\bar{X}}_{i1} = \bar{V}_{i1}, \\ \dot{\bar{X}}_{i2} = \bar{V}_{i2}, \end{cases} \tag{5.21}$$

where

$$g(t) := N \int_0^t \bar{C}(t-\tau)\, d\tau.$$

Now we will prove the uniform asymptotic stability of equilibrium (5.16) providing a suitable Lyapunov function for system (5.21). For simplicity, system (5.21) can be written, for each particle and for each component, as a planar system in the variable $\mathbf{y} = (V, X)$:

$$\begin{cases} \dot{V} = -\beta V - g(t)X, \\ \dot{X} = V, \end{cases} \tag{5.22}$$

with

$$g(t) := N \int_0^t \bar{C}(t-\tau)\, d\tau. \tag{5.23}$$

In relation to (5.22) we prove the following two theorems.

Theorem 3. *Fixed a $\bar{t} > 0$, the system (5.22), admits a Lyapunov function $U(t, \mathbf{y})$ with the properties:*

a)

$$k_2 \|\mathbf{y}\|^2 \leq U(t, \mathbf{y}) \leq k_1 \|\mathbf{y}\|^2 ; \tag{5.24}$$

b)

$$\dot{U}(t, \mathbf{y}) = \frac{\partial U}{\partial t} + \frac{\partial U}{\partial V}\dot{V} + \frac{\partial U}{\partial X}\dot{X} \leq -k_3 \|\mathbf{y}\|^2 ; \tag{5.25}$$

for all $t \geq \bar{t}$, where k_1, k_2, and k_3 are positive constants.

Proof. Let $\bar{t} > 0$, we define the Lyapunov function

$$U(t, V, X) := (V^2 + kXV + g(t)X^2)\psi(t),$$

where

$$\psi(t) := e^{-\frac{g(t)}{\underline{g}}}, \tag{5.26}$$

$$\underline{g} := \inf_{t\geq \bar{t}} g(t) = N\int_0^{\bar{t}} \bar{C}(t-\tau)\,d\tau, \quad \overline{g} := \sup_{t\geq \bar{t}} g(t) = N\int_0^{+\infty} \bar{C}(t-\tau)\,d\tau, \tag{5.27}$$

$$\underline{\psi} := \inf_{t\geq \bar{t}} \psi = e^{-\frac{\bar{g}}{\underline{g}}}, \quad \overline{\psi} := \sup_{t\geq \bar{t}} \psi = e^{-1}, \tag{5.28}$$

$$\overline{\overline{\psi}} := \sup_{t\geq \bar{t}} |\dot{\psi}| = \sup_{t\geq \bar{t}} \frac{e^{-\frac{g(t)}{\underline{g}}}\dot{g}}{\underline{g}}, \tag{5.29}$$

$$k := \min\left[\frac{\underline{\psi}}{\overline{\overline{\psi}}}, \frac{\underline{g}\,\underline{\psi}}{\overline{\overline{\psi}}}, \frac{2\beta\underline{g}\,\underline{\psi}^2}{2\underline{g}\,\underline{\psi}\overline{\psi} + (\overline{\overline{\psi}} + \beta\overline{\psi})^2}\right]. \tag{5.30}$$

In the following equations we consider the inequalities:

$$-\frac{X^2+V^2}{2} \leq XV \leq \frac{X^2+V^2}{2}.$$

Then, because of $g(t)$ is an increasing function, $\psi(t)$ is nonincreasing, so

$$\dot{\psi} \leq 0, \tag{5.31}$$

and finally

$$\begin{aligned} \dot{\psi}g + \psi\dot{g} &= -e^{-\frac{g(t)}{\underline{g}}}\frac{\dot{g}}{\underline{g}}g + e^{-\frac{g(t)}{\underline{g}}}\dot{g} \\ &= \dot{g}e^{-\frac{g(t)}{\underline{g}}}\left(1 - \frac{g(t)}{\underline{g}}\right) \\ &\leq 0, \quad \forall\, t \geq \bar{t}. \end{aligned} \tag{5.32}$$

To prove the second inequality in a) we consider

$$\begin{aligned} U(t,V,X) &\leq \left(V^2 + k\frac{X^2+V^2}{2} + \overline{g}X^2\right)\overline{\psi} \\ &= \left[\left(1+\frac{k}{2}\right)V^2 + \left(\overline{g} + \frac{k}{2}\right)X^2\right]\overline{\psi} \\ &\leq k_1\left\|\mathbf{y}\right\|^2, \end{aligned}$$

where

$$k_1 := \max\left[\left(1+\frac{k}{2}\right)\overline{\psi}, \left(\overline{g}+\frac{k}{2}\right)\overline{\psi}\right].$$

To prove the first part of a) we consider

$$\begin{aligned} U(t,V,X) &\geq \underline{\psi}V^2 + \underline{g}\,\underline{\psi}X^2 - k\overline{\psi}\frac{X^2+V^2}{2} \\ &= V^2\left(\underline{\psi} - \frac{k\overline{\psi}}{2}\right) + X^2\left(\underline{g}\,\underline{\psi} - \frac{k\overline{\psi}}{2}\right) \\ &\geq_{(5.30)} V^2\frac{\underline{\psi}}{2} + X^2\frac{\underline{g}\,\underline{\psi}}{2} \\ &\geq k_2\left\|\mathbf{y}\right\|^2, \end{aligned}$$

where

$$k_2 := \min\left[\frac{\underline{\psi}}{2}, \frac{\underline{g}\,\underline{\psi}}{2}\right]$$

To prove b) we consider the following inequalities:

$$\begin{aligned} \dot{U}(t,V,X) &= \dot{\psi}(V^2 + kXV + gX^2) + \psi\left[2V(-\beta V - gX) + kV^2\right. \\ &\left. +kX(-\beta V - gX) + \dot{g}X^2 + 2gXV\right] \\ &= \left(\dot{\psi} - 2\beta\psi + k\psi\right)V^2 + \left(k\dot{\psi} - \beta k\psi\right)XV + \left(\dot{\psi}g + \psi\dot{g} - kg\psi\right)X^2 \\ &\leq_{(5.31),(5.32)} \left(-2\beta\psi + k\psi\right)V^2 + \left(k\dot{\psi} - \beta k\psi\right)XV - kg\psi X^2 \\ &\leq \left(-2\beta\psi + k\psi\right)V^2 + \left(k|\dot{\psi}| + \beta k\psi\right)|X||V| - kg\psi X^2 \\ &\leq \left(-2\beta\underline{\psi} + k\overline{\psi}\right)V^2 + \left(k\overline{\overline{\psi}} + \beta k\overline{\psi}\right)|X||V| - k\underline{g}\,\underline{\psi}X^2 \\ &= \left(-2\beta\underline{\psi} + k\overline{\psi}\right)V^2 - \frac{k\underline{g}\,\underline{\psi}}{2}\left[|X| - \frac{|V|\left(\overline{\overline{\psi}} + \beta\overline{\psi}\right)}{\underline{g}\,\underline{\psi}}\right]^2 - \frac{k\underline{g}\,\underline{\psi}}{2}X^2 \\ &+ \frac{k\left(\overline{\overline{\psi}} + \beta\overline{\psi}\right)^2}{2\underline{g}\,\underline{\psi}}V^2 \\ &\leq \left(-2\beta\underline{\psi} + k\overline{\psi} + \frac{k\left(\overline{\overline{\psi}} + \beta\overline{\psi}\right)^2}{2\underline{g}\,\underline{\psi}}\right)V^2 - \frac{k\underline{g}\,\underline{\psi}}{2}X^2 \\ &\leq_{(5.30)} -\left(\beta\underline{\psi}V^2 + \frac{k\underline{g}\,\underline{\psi}}{2}X^2\right) \\ &\leq -k_3\left\|\mathbf{y}\right\|^2, \end{aligned}$$

where

$$k_3 := \min\left[\beta\underline{\psi}, \frac{k\underline{g}\,\underline{\psi}}{2}\right].$$

This completes the proof.

Starting from Theorem 3 we can state

Theorem 4. *The equilibrium point* $(V, X) = (0, 0)$ *of the linearized system* (5.22) *is globally uniformly asymptotically stable with exponential rate of convergence.*

Proof. Inequalities (5.25) and (5.24) imply that U satisfies the differential inequality

$$\dot{U} \leq -\frac{k_3}{k_1} U, \quad \forall\, t \geq \bar{t}.$$

By the Gronwall's inequality,

$$U(t, \mathbf{y}(t)) \leq U\left(\bar{t}, \mathbf{y}\left(\bar{t}\right)\right) e^{-(k_3/k_1)(t-\bar{t})}.$$

Then, using again (5.24), we have

$$\begin{aligned} \|\mathbf{y}(t)\| &\leq \left(\frac{U(t, \mathbf{y}(t))}{k_2}\right)^{1/2} \\ &\leq \left(\frac{U\left(\bar{t}, \mathbf{y}\left(\bar{t}\right)\right) e^{-(k_3/k_1)(t-\bar{t})}}{k_2}\right)^{1/2} \\ &\leq \left(\frac{k_1 \left\|\mathbf{y}\left(\bar{t}\right)\right\|^2 e^{-(k_3/k_1)(t-\bar{t})}}{k_2}\right)^{1/2} \\ &= \left(\frac{k_1}{k_2}\right)^{1/2} \left\|\mathbf{y}\left(\bar{t}\right)\right\| e^{-(k_3/(2k_1))(t-\bar{t})}. \end{aligned} \tag{5.33}$$

From (5.33) conditions for the uniform asymptotic stability are satisfied with exponential convergence. The proof is completed.

Returning to system (5.21), Theorem 4 can be applied for each particle and for each component of the position and velocity vectors. Recalling transformations (5.14)–(5.15), we can say that all agents converge, time-asymptotically, to the position and velocity of their centre of mass.

Now, let us investigate equation (5.19) for the motion of the centre of mass. For convenience, we write it again for the first component, the second is similar:

$$\begin{cases} \dot{V}_{\mathrm{CM1}} = -N \displaystyle\int_0^t \bar{C}(t-\tau) \left(X_{\mathrm{CM},1}(t) - X_{\mathrm{CM1}}(\tau)\right) d\tau, \\ \dot{X}_{\mathrm{CM1}} = V_{\mathrm{CM1}}, \end{cases} \tag{5.34}$$

with $\bar{C}(t-\tau)$ defined in (5.10) that, from (5.2), gives

$$\bar{C}(t-\tau) := \frac{\pi R^2 C(t-\tau) e^{-\frac{R^2}{4(t-\tau)D}}}{2(t-\tau)D} = \frac{\gamma \xi R^2 e^{-\frac{R^2}{4(t-\tau)D} - \eta(t-\tau)}}{8(t-\tau)^2 D^2}. \tag{5.35}$$

Then from system (5.34) we get the scalar equation

$$\dot{V}_{\mathrm{CM1}} = -N \int_0^t \bar{C}(t-\tau) \int_\tau^t V_{\mathrm{CM1}}(s)\, ds\, d\tau, \tag{5.36}$$

and similarly

$$\dot{V}_{\mathrm{CM2}} = -N \int_0^t \bar{C}(t-\tau) \int_\tau^t V_{\mathrm{CM2}}(s)\, ds\, d\tau. \tag{5.37}$$

In order to establish the asymptotic behaviour of (5.36), we prove the following

Theorem 5. *Equation* (5.36)*, with initial datum* $V_{CM1}(t_0)$*, has a unique solution in* $[t_0, +\infty)$*.*

Proof. The existence of the solution is ensured by the existence of the solution proved for system (5.1).

Since the linearity of the equation it is enough to prove that the unique solution with zero initial datum is the constant zero solution. In fact, if we consider the case of nonzero initial datum and we suppose that there exist two solutions, $y(t)$ and $z(t)$, in correspondence of the same initial condition $y(t_0) = z(t_0)$, their difference $w(t) := y(t) - z(t)$ is also a solution with zero initial datum. If $w(t)$ must be necessarily the zero solution, then $y(t)$ and $z(t)$ have to coincide, ensuring the uniqueness.

First, we observe that $\bar{C}(t-\tau)$ in (5.35) is bounded, we say

$$0 < N\bar{C}(t-\tau) \leq \nu,$$

with ν positive constant. Then, from (5.36) we write the inequalities

$$\begin{aligned}\frac{d\,|V_{\mathrm{CM1}}|}{dt} &\leq \left|\frac{dV_{\mathrm{CM1}}}{dt}\right| \\ &\leq \nu \int_0^t \int_\tau^t |V_{\mathrm{CM1}}(s)|\; ds\, d\tau \\ &= \nu \int_0^t s\,|V_{\mathrm{CM1}}(s)|\; ds,\end{aligned}$$

where we have changed the order of integration in the integrals. Integrating both sides from t_0 to t, changing again the order of integration, and fixed a $T > t_0$, we state

$$\begin{aligned}|V_{\mathrm{CM1}}(t)| &\leq |V_{\mathrm{CM1}}(t_0)| + \nu \int_{t_0}^t \int_0^\tau s\,|V_{\mathrm{CM1}}(s)|\; ds\, d\tau \\ &\leq |V_{\mathrm{CM1}}(t_0)| + \nu \int_0^t \int_0^\tau s\,|V_{\mathrm{CM1}}(s)|\; ds\, d\tau \\ &= |V_{\mathrm{CM1}}(t_0)| + \nu \int_0^t s(t-s)\,|V_{\mathrm{CM1}}(s)|\; ds \\ &\leq |V_{\mathrm{CM1}}(t_0)| + \nu T \int_0^t s\,|V_{\mathrm{CM1}}(s)|\; ds, \quad \forall t_0 \leq t < T.\end{aligned}$$

By Gronwall's Lemma

$$|V_{\mathrm{CM1}}(t)| \leq |V_{\mathrm{CM1}}(t_0)|\, e^{\frac{\nu T t^2}{2}}, \quad \forall t_0 \leq t < T,$$

so that, due to the arbitrariness of T, if $V_{\mathrm{CM1}}(t_0) = 0$, $V_{\mathrm{CM1}}(t)$ will be the constant zero solution. This completes the proof.

From Theorem 5 descends

Theorem 6. *Each solution of equation* (5.36) *tends to zero as* $t \to +\infty$*.*

Proof. If the initial datum is $V_{\mathrm{CM1}}(0) = 0$ the unique solution is the constant zero solution. We consider now $V_{\mathrm{CM1}}(0) > 0$. In this case the solution is greater or equal to zero in all $[0, +\infty)$. In fact, if there is a $\bar{t} > 0$ such that $V_{\mathrm{CM1}}(\bar{t}) = 0$, Theorem 5, applied at $t_0 = \bar{t}$, would give $V_{\mathrm{CM}1}(t) \equiv 0$ for all $t > \bar{t}$. Then the right hand side of (5.36) implies $\dot{V}_{\mathrm{CM}1} < 0$, so $V_{\mathrm{CM}1}(t)$ is a decreasing function on $[0, +\infty)$, and there exits its limit $0 \le l < +\infty$, as $t \to +\infty$. Hence, since from (5.36) $\dot{V}_{\mathrm{CM}1}(t)$ is monotone and its limit exists, we have also $\lim_{t\to+\infty} \dot{V}_{\mathrm{CM}1}(t) = 0$. Now, if we suppose $l > 0$, $V_{\mathrm{CM}1}(t) > l$ for all $t \ge 0$, and from (5.36) holds

$$\dot{V}_{\mathrm{CM}1} < -Nl \int_0^t \bar{C}(t-\tau)(t-\tau)\,d\tau \tag{5.38}$$

$$= -Nl \int_0^t z\bar{C}(z)\,dz, \quad \forall t \in [0, +\infty), \tag{5.39}$$

where we have performed the change of variables $z = t - \tau$. Taking the limit for $t \to +\infty$ on both sides of (5.38) we would have the contradiction

$$0 = \lim_{t\to+\infty} \dot{V}_{\mathrm{CM}1}(t) \le -\mu < 0,$$

where

$$\mu := Nl \int_0^{+\infty} z\bar{C}(z)\,dz.$$

So the only chance is $l = 0$.

The case $V_{\mathrm{CM}1}(0) < 0$ can be treated in a similar way. The proof is now completed.

Theorem 6 is valid also for the second velocity component $V_{\mathrm{CM}2}$, whose equation is analogous to (5.36).

Finally, returning to system (5.11), Theorems 6 and 4 ensure a condition of time-asymptotic flocking such as stated in Definition 1. Moreover, we have also the stronger condition that all particles converge asymptotically to their centre of mass and the velocity of the centre of mass decays to zero.

6. Numerical simulations

In this section we present some numerical simulations to show the dynamical behaviour of the model introduced in Section 2. Numerical results are compared with the analytical ones presented in Section 3 and some similar cases are considered.

Numerical tests are performed and shown in nondimensional form using the following dimensionless quantities:

$$t^* := t\eta, \quad \mathbf{X}^* := \frac{\mathbf{X}}{R}, \quad f^* := \frac{f}{f_{\max}}, \quad \beta^* := \frac{\beta}{\eta},$$
$$\gamma^* := \frac{\gamma f_{\max}}{R^2\eta^2}, \quad D^* := \frac{D}{R^2\eta}, \quad \xi^* := \frac{\xi}{f_{\max}\eta},$$

where $f_{\max}$ is the maximum concentration of signal f. With these definitions, system (2.1) can be written as

$$\begin{cases} \dot{\mathbf{V}}_i = \dfrac{\beta}{N} \displaystyle\sum_{j=1}^{N} \dfrac{1}{\left(1 + \|\mathbf{X}_i - \mathbf{X}_j\|^2\right)^{\sigma}} (\mathbf{V}_j - \mathbf{V}_i) + \gamma \nabla f(\mathbf{X}_i), \\ \\ \dot{\mathbf{X}}_i = \mathbf{V}_i, \\ \\ \partial_t f = D \Delta f + \xi \displaystyle\sum_{j=1}^{N} \chi_{\mathbf{B}(\mathbf{X}_j, 1)} - f, \end{cases} \tag{6.1}$$

where we have dropped, for simplicity, the asterisks for the nondimensional quantities. Notice that, due to the choice of R as characteristic length, the dimensionless particle ray turns out to be a unit value.

6.1. **Numerical methods.** The numerical approximation scheme used here employs a 2D finite difference method on a spatial domain $\Omega := [a, b] \times [c, d]$ with periodic boundary conditions.

For the parabolic equation $(6.1)_3$, in order to eliminate the stiff term $-f$ we perform the classic exponential transformation, and we apply a central difference scheme in space and the parabolic Crank-Nicolson scheme in time.

For equations $(6.1)_1$ we adopt a one step IMEX method, putting in implicit the term depending on the velocities and in explicit the gradient term (Hundsdorfer and Verwer, 2003).

For further details we refer to Appendix A.

6.2. **Numerical tests.** In all the following numerical tests we set N particles in a spatial domain $\Omega = [0, 50] \times [0, 50]$ with periodic boundary conditions, and we choose a suitable time interval of observation $[0, T]$. For the initial data we fix

$$f(\mathbf{x}, 0) = 0,$$

and, for $i = 1, \dots, N$,

$$\mathbf{X}_i(0) = \mathbf{X}_{i0},$$
$$\mathbf{V}_i(0) = \mathbf{V}_{i0}.$$

In particular $\mathbf{X}_{i0}$ is chosen as a random vector, such that all the particles at $t = 0$ are contained in a suitable initial region, fixed in the domain. Then $\mathbf{V}_{i0} = (V_{i0} \cos\theta_i, V_{i0} \sin\theta_i)$ are chosen with V_{i0} random numbers in $[0, V_{0,\max}]$, and θ_i random numbers in $[0, 2\pi]$. Let us now describe some meaningful tests.

Test 1. In this test we set the parameters $\sigma = 0.5$, $\beta = 5$, $\gamma = 2 \times 10^2$, $D = 2 \times 10^2$, $\xi = 0.5$, $V_{0,\max} = 3$, and we consider $N = 10$ particles located in $\mathbf{X}_0$ as in Figure 6.1 (a). The time interval of observation is $[0, 500]$. Spatial and temporal discretizations are given respectively by $\Delta x = \Delta y = 0.25$ and $\Delta t = 10^{-4}$.

Figure 6.1 shows four time steps of the numerical simulation. Here and in the next tests for each time step we plot, on the left the chemoattractant concentration $f(\mathbf{x}, t)$, while on the right the positions and the velocities of the particles in the spatial domain. The red square at $t = 0$ is the region in which the initial positions are taken. The red marker indicates the centre of mass of the system, and the blue arrows are the velocity vectors. We observe an initial stage in which the particles tend to move somewhat aligned about until $t = 5$ (Figure 6.1 (b)), then they begin to converge to their centre of mass about at $t = 30$ (Figure 6.1 (c)), finally all particles stop in a same position (Figure 6.1 (d)).

In Figure 6.2 (a) is shown the spatial fluctuation around the centre of mass system

$$Fl_X(t) := \sum_{i=1}^{N} \|\mathbf{X}_i(t) - \mathbf{X}_{\mathrm{CM}}(t)\|^2 ,$$

as a function of the time. In Figure 6.2 (b) is shown the velocity fluctuation around the centre of mass

$$Fl_V(t) := \sum_{i=1}^{N} \|\mathbf{V}_i(t) - \mathbf{V}_{\mathrm{CM}}(t)\|^2 .$$

For $t \geq 61$ $Fl_X(t)$ and $Fl_V(t)$ are less than 10^{-10}. Notice that the square root of $Fl_X(t)$ and $Fl_V(t)$ is proportional to the standard deviations of $\mathbf{X}_i(t)$ and $\mathbf{V}_i(t)$ with respect to the position and velocity of the centre of mass. Figure 6.2 (c) displays the norm of the velocity of the centre of mass $\|\mathbf{V}_{\mathrm{CM}}(t)\|$ versus time. For $t \geq 52$ this velocity is less than 7.8×10^{-2}. The oscillating pattern, shown here and in the next tests, can be attributed to the numerical error, as it is confirmed using finer meshes for the discretization. Figure 6.2 (d) is obtained, for the same simulation, using a spatial and temporal steps respectively of $\Delta x = \Delta y = 0.0125$ and $\Delta t = 10^{-5}$. For $t \geq 88$ $\|\mathbf{V}_{\mathrm{CM}}(t)\|$ is less than 2×10^{-2}. With smaller values of Δx, Δy, and Δt, lower values of $\|\mathbf{V}_{\mathrm{CM}}(t)\|$ are achieved (data not shown).

In the next two tests, starting from Test 1, we change only the two parameters related to the alignment and to the chemotaxis, in order to investigate the competition between these two effects.

Test 2. In this test we set $\beta = \gamma = 10$, while the other parameters are set as in Test 1. The time of observation is $[0, 3500]$.

Particles and chemotactic signal are not shown. In Figure 6.3 (a)–(b) we plot the spatial and the velocity fluctuations around the centre of mass system $Fl_X(t)$ and $Fl_V(t)$. For $t \geq 1689$ $Fl_X(t)$ and $Fl_V(t)$ are less than 10^{-10}. Figure 6.3 (c) displays the quantity $\|\mathbf{V}_{\mathrm{CM}}(t)\|$ as a function of time. For $t \geq 2134$ this value is less than 1.82×10^{-2}.

Test 3. In this test we set $\beta = 15$, $\gamma = 10$ and the other parameters are set as in Test 1. The time of observation is $[0, 3500]$.

The figures related to the particles and to the chemotactic signal are not shown, while in Figure 6.4 (a)–(b) we plot the spatial and the velocity fluctuations around the centre of mass system $Fl_X(t)$ and $Fl_V(t)$. For $t \geq 3109$ we have values less than 10^{-10}. Figure 6.4 (c) displays the quantity $\|\mathbf{V}_{\mathrm{CM}}(t)\|$ versus time. For $t \geq 2579$ this velocity is less than 1.87×10^{-2}.

In Table 1 we summarize the results of the first three tests. We can observe that increasing values of the ratio $\frac{\beta}{\gamma}$ imply a decreasing rate of convergence of the particles.

TABLE 1. Spatial and velocity fluctuations in the centre of mass system, and velocity of the centre of mass for different values of the parameters β and γ used in Tests 1–3.

Test	β	γ	Time after which $\max\{Fl_X, Fl_V\} < 10^{-10}$	Time after which $\|\mathbf{V}_{\mathrm{CM}}(t)\| < 7.8 \times 10^{-2}$
1	5	2×10^2	61	52
2	10	10	1689	1021
3	15	10	3109	1554

Test 4. In this simulation we fix the parameters as in Test 1, and we double the number of the interacting agents, considering $N = 20$ cells as in Figure 6.5 (a). The time interval of observation is $[0, 500]$.

In Figure 6.5 we can observe four different time steps of the numerical simulation showing the aggregation of the initial group and the convergence to zero of its velocity.

In Figures 6.6 (a)–(b) we plot, the quantities $Fl_X(t)$ and $Fl_V(t)$. Here, for $t \geq 34$ we have values less than 10^{-10}. In Figure 6.6 (c) we show the quantity $\|\mathbf{V}_{\mathrm{CM}}(t)\|$ versus time, with values smaller than 8.39×10^{-2} for $t \geq 28$. Comparing the results of this test with those of Test 1 we can state that, with the same parameters, an increasing number of cells enhances the rate of convergence due to the greater amount of the expressed chemoattractant.

Test 5. In this test we consider a case in which, for the pure Cucker-Smale model (1.1), i.e. $\gamma = 0$ in our model, the flocking behaviour does not occur. We fix the other parameters $\sigma = 0.8$, $\beta = 5$, $D = 2 \times 10^2$, $\xi = 0.5$, $V_{0,\max} = 3$, and $\mathbf{X}_0$ as in Figure 6.7 (a). The time interval of observation is $[0, 15]$. Spatial and temporal discretizations are as in Test 1. Clearly in this case equations $(6)_{1,2}$ and $(6)_3$ are decoupled. Since $\sigma > 1/2$, and taking into account the initial data, according to the results in Ha and Liu (2009), the flocking of the system is not guaranteed.

Figure 6.7 shows our numerical simulation at three time steps. We can observe, in fact, a dispersion of the initial group of particles.

In the next test we will show that, adding the chemotactic effect, we can recover the time-asymptotic convergence of the migrating group.

Test 6. In this test we set the same parameters and initial data of Test 5, moreover we introduce a non zero value for the chemotactic effect: $\gamma = 10^2$. The interval of observation, spatial and temporal discretizations are fixed as in Test 1.

Figure 6.8 shows the numerical simulations at four different time steps. We can note that the initial group of particles does not disperse, but converge in position and velocity.

In Figures 6.9 (a)–(b) we plot, as in Test 1, respectively $Fl_X(t)$ and $Fl_V(t)$. For $t \geq 107$ these quantities are less than 10^{-10}. Figure 6.9 (c) shows the quantity $\|\mathbf{V}_{\mathrm{CM}}(t)\|$ versus time. For $t \geq 65$ we have values smaller than 2.1×10^{-2}.

Test 7. Inspired by the mathematical model proposed in Di Costanzo et al (2015) for the zebrafish lateral line development, we consider a simulation in which two kinds of cells are involved: the *leaders* that produce the chemotactic signal and the *followers* that do not produce any signal, both subjected to the alignment effect and to the attraction of the chemical gradient.

For the numerical simulation set $\sigma = 0.5$, $\beta = 5$, $\gamma = 1.5 \times 10^2$, $D = 2 \times 10^2$, $\xi = 3$, $V_{0,\max} = 0.3$, and $\mathbf{X}_0$ as in Figure 6.10 (a). We consider a time interval of observation $[0, 500]$. Spatial and temporal discretizations are as in Test 1.

Figure 6.10 shows four time steps of our simulation. A single leader cell is marked in green colour, while the other follower cells are in red colour. Here the centre of mass is marked in blue. We observe, about at $t = 15$, that cells begin to be attracted toward the chemoattractant source (Figure 6.10 (b)). In the next time steps the cells tend to converge in the centre of mass and then they stop (Figure 6.10 (c)–(d)).

In Figures 6.11 (a)–(b) are shown the spatial and velocity fluctuations, $Fl_X(t)$ and $Fl_V(t)$, around the centre of mass system. For $t \geq 131$ these quantities are less than 10^{-10}. Figure 6.11 (c) displays the quantity $\|\mathbf{V}_{\mathrm{CM}}(t)\|$. For $t \geq 328$ we have values smaller than 5.3×10^{-2}.

Test 8. In this test we consider a case in which the particles have zero initial velocity. If we considered the pure Cucker-Smale model (1.1), we would have the particles constant in the initial position with zero velocity. Here we show that the chemotactic effect ensure the convergence of the group of particles. As in Test 7 we consider a single leader that produce the chemoattractant, and other followers that do not produce any signal, but they follow the gradient produced by the leader signal.

For the numerical simulation we set $\sigma = 0.6$, $\beta = 2$, $\gamma = 10^2$, $D = 2 \times 10^2$, $\xi = 3$, $V_{0,\max} = 0$, and $\mathbf{X}_0$ as in Figure 6.12 (a). The time interval of observation is the same as Test 5. Spatial and temporal discretizations are fixed as in Test 1.

Figure 6.12 shows four time steps of our simulation. Green colour marks the leader cell, while red colour is for the followers. The centre of mass is marked in blue. In early time steps we observe the velocity vectors that point the source of chemoattractant (Figure 6.12 (b)). In the next time steps all particles go to converge in position and velocity.

In Figures 6.13 (a)–(b) we plot respectively $Fl_X(t)$ and $Fl_V(t)$ versus time. For $t \geq 67$ we obtain values less than 10^{-10}. In Figure 6.13 (c) is shown the quantity $\|\mathbf{V}_{\mathrm{CM}}(t)\|$ as a function of time. For $t \geq 109$ we have values smaller than 4.3×10^{-2}.

Test 9. In this test we simulate the system only under the chemotactic effect, neglecting the alignment term, that is we set $\beta = 0$. The other parameters are $\gamma = 10^2$, $D = 2 \times 10^2$, $\xi = 1.5$, and the initial data $V_{0,\max} = 0.8$, $\mathbf{X}_0$ as in Figure 6.14 (a). The time interval of observation is $[0, 4000]$. Spatial and temporal discretizations are fixed as in Test 1.

In Figure 6.14 we plot four time steps. Although the initial group aggregates, we do not observe, in our time of observation, a convergence of the particles, rather they show an oscillating behaviour around their centre of mass.

In Figures 6.15 (a)–(b) we plot respectively $Fl_X(t)$ and $Fl_V(t)$. In this case, the spatial and velocity fluctuations around the centre of mass remain bounded but do not converge to zero. In particular, in the time interval of observation, we have $Fl_X(t) \geq 0.88$ and, if we consider a trend line, its slope seems to decreases monotonically approaching to zero. For example, in relation to Figure 6.15 (a), the slope of the linear fit on the values of $Fl_X(t)$, computed on the time intervals $[0, 800]$ and $[3200, 4000]$, changes from -1.46×10^{-1} to -1.84×10^{-4}. Moreover, we remark that in previous simulations, containing the alignment effect, on time intervals much smaller than this test we have obtained values of $Fl_X(t)$ less than 10^{-10}.

In Figure 6.15 (c) is shown $\|\mathbf{V}_{\mathrm{CM}}(t)\|$ as a function of time. For $t \geq 254$ we have values smaller than 3.79×10^{-2}. Performing the same numerical test with the finer discretization $\Delta x = \Delta y = 1.25$ and $\Delta t = 10^{-5}$, we find that, for $t \geq 120$, $\|\mathbf{V}_{\mathrm{CM}}(t)\|$ is smaller than 1.41×10^{-2}, see Figure 6.15 (d). From this we can deduce that the velocity of the centre of mass goes to zero.

Our numerical results suggest that our model, in absence of alignment and with the only chemotactic effect, is unable to reproduce stationary patterns.

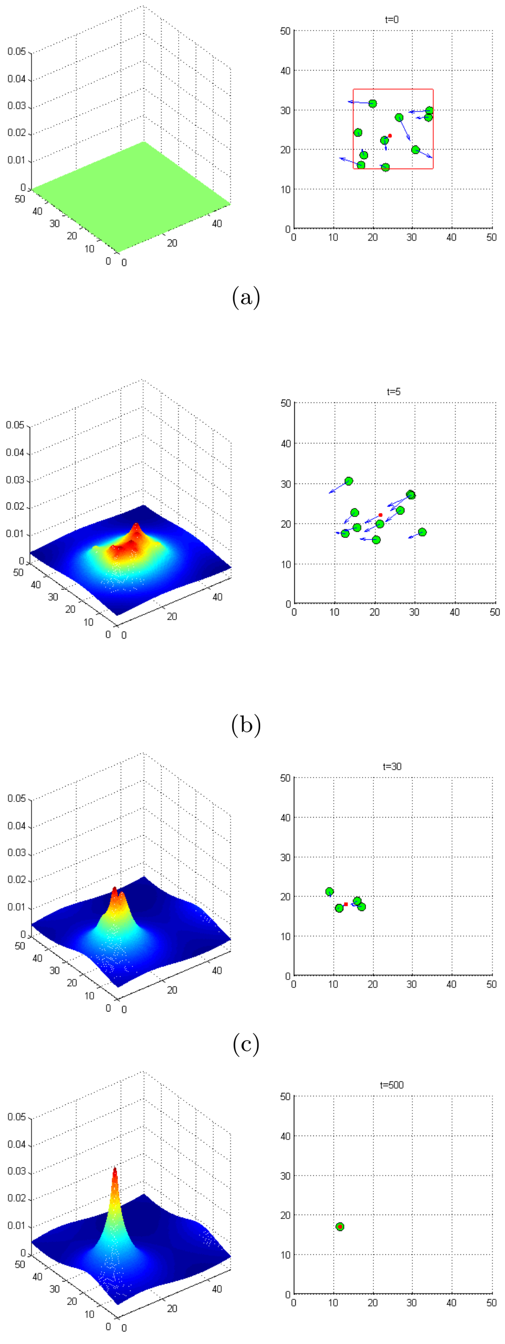

(a)

(b)

(c)

(d)

Figure 6.1. **Test 1**. Numerical simulation in a spatial domain $\Omega = [0,50] \times [0,50]$ with periodic boundary conditions, and in the time interval $[0,500]$. The parameters values are $\sigma = 0.5$, $\beta = 5$, $\gamma = 2 \times 10^2$, $D = 2 \times 10^2$, $\xi = 0.5$, $V_{0,\max} = 3$, and $\mathbf{X}_0$ randomly taken in the red square shown in (a). Spatial and temporal discretizations are respectively $\Delta x = \Delta y = 0.25$ and $\Delta t = 10^{-4}$. The four plots are respectively at time steps $t = 0, 5, 30, 500$. On the left there is the chemoattractant concentration $f(\mathbf{x}, t)$, while on the right the positions and the velocities of the particles. The red marker indicates the centre of mass of the system, and the blue arrows are the velocity vectors.

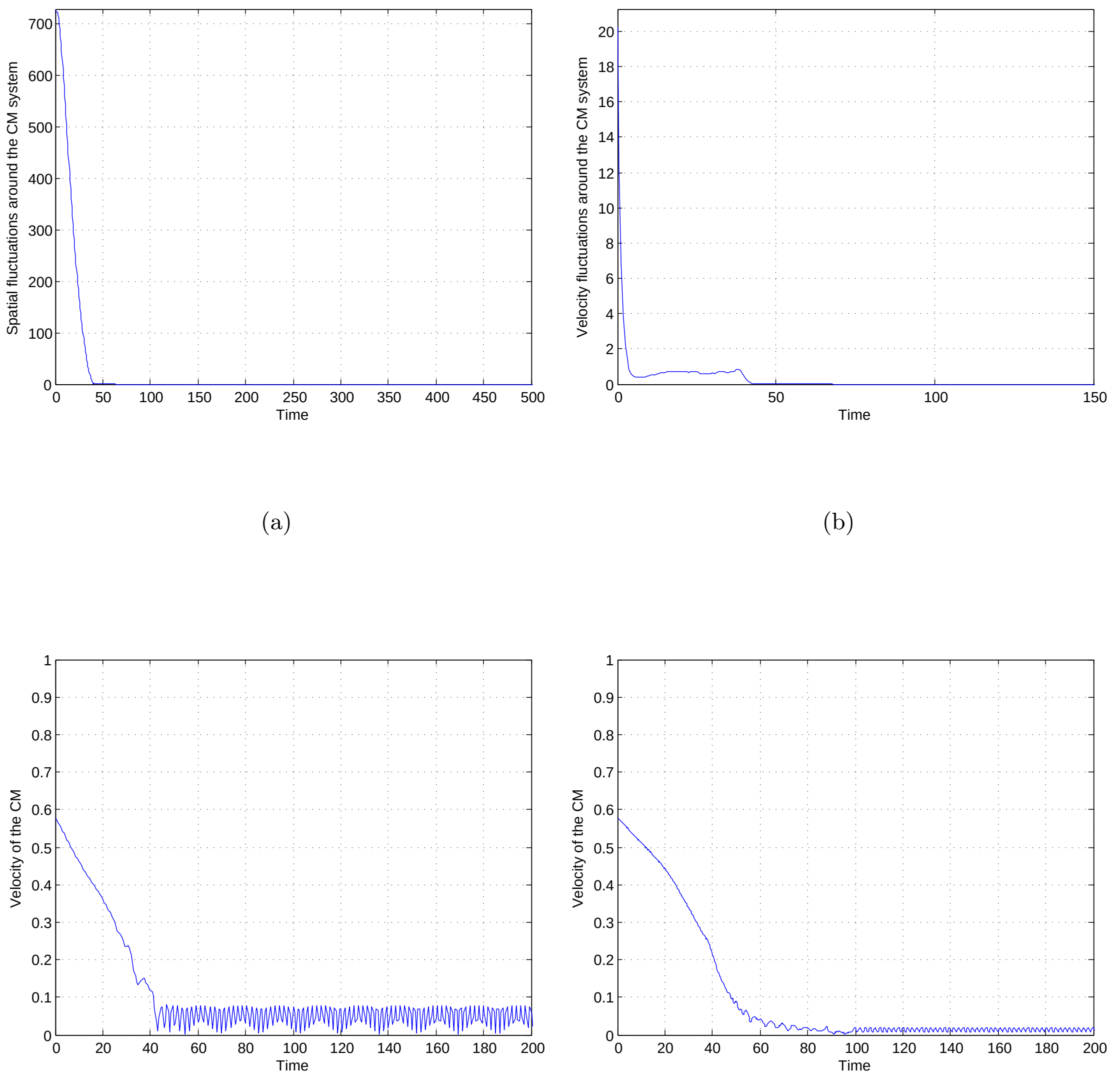

(a) (b)

(c) (d)

FIGURE 6.2. **Test 1**. (a) Spatial fluctuation around the centre of mass system $Fl_X(t) := \sum_{i=1}^{N} \|\mathbf{X}_i(t) - \mathbf{X}_{\mathrm{CM}}(t)\|^2$ as a function of the time. (b) Velocity fluctuation around the centre of mass system $Fl_V(t) := \sum_{i=1}^{N} \|\mathbf{V}_i(t) - \mathbf{V}_{\mathrm{CM}}(t)\|^2$ as a function of the time (x-axis shows only a part of the time domain). For $t \geq 61$ $Fl_X(t)$ and $Fl_V(t)$ are less than 10^{-10}. (c) Norm of the velocity of the centre of mass $\|\mathbf{V}_{\mathrm{CM}}(t)\|$ versus time (only a part of the time interval is shown on the x-axis). For $t \geq 52$ this velocity is less than 7.8×10^{-2}. The plot is related to a numerical simulation with spatial and temporal steps respectively of $\Delta x = \Delta y = 0.25$ and $\Delta t = 10^{-4}$. (d) With a finer mesh, $\Delta x = \Delta y = 0.125$ and $\Delta t = 10^{-5}$, smaller values of $\|\mathbf{V}_{\mathrm{CM}}(t)\|$ can be obtained: for $t \geq 88$ the maximum value in the plot is less than 2×10^{-2}. This confirm that the oscillating pattern shown in (c) can be attributed to a numerical error.

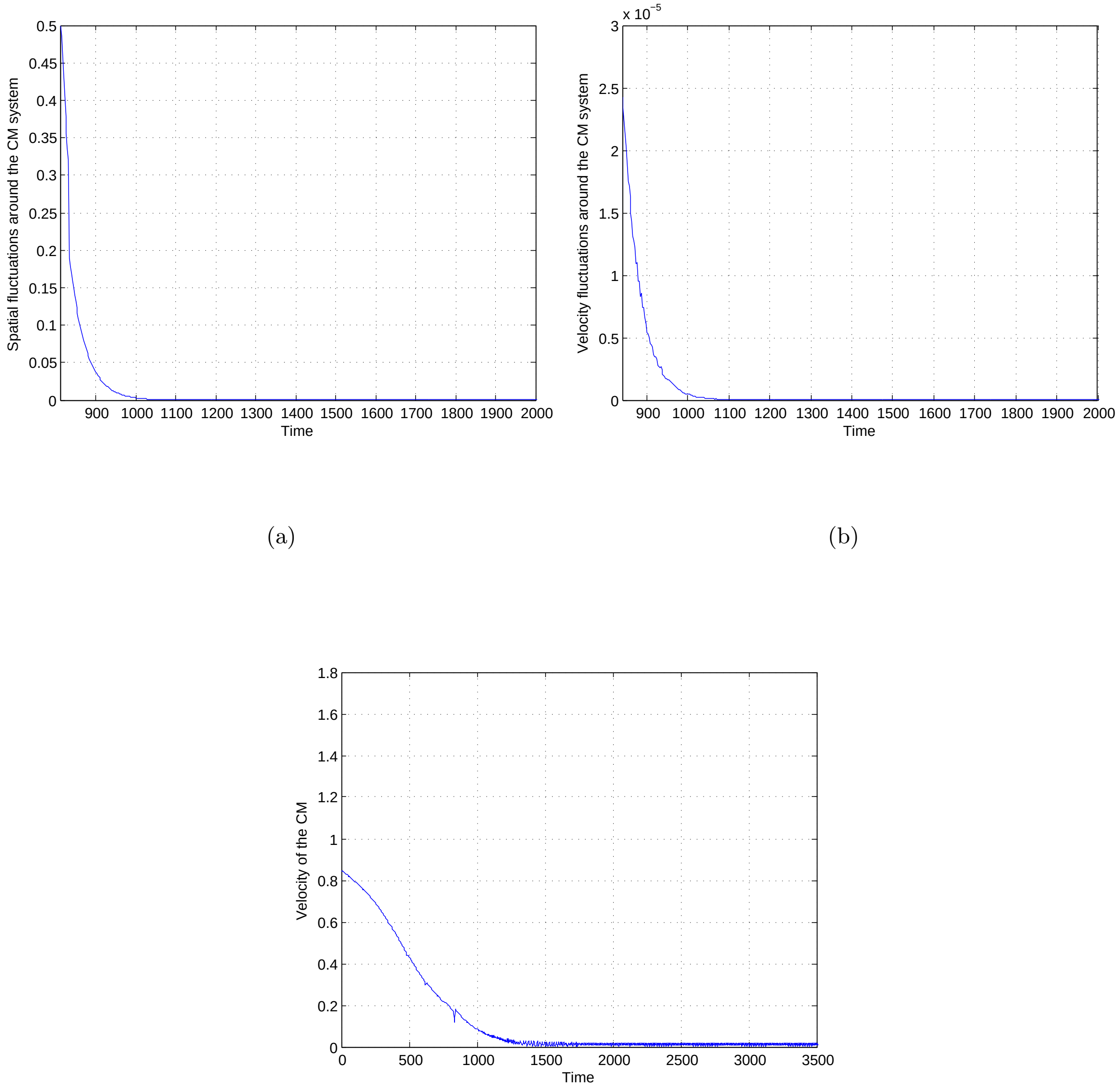

(a) (b)

(c)

FIGURE 6.3. **Test 2**. (a)-(b) Spatial and velocity fluctuations around the centre of mass system $Fl_X(t)$ and $Fl_V(t)$. For $t \geq 1689$ $Fl_X(t)$ and $Fl_V(t)$ are less than 10^{-10} (on the x-axis only a part of the time domain is shown). (c) Norm of the velocity of the centre of mass $\|\mathbf{V}_{\mathrm{CM}}(t)\|$ versus time. For $t \geq 2134$ this velocity is less than 1.82×10^{-2}.

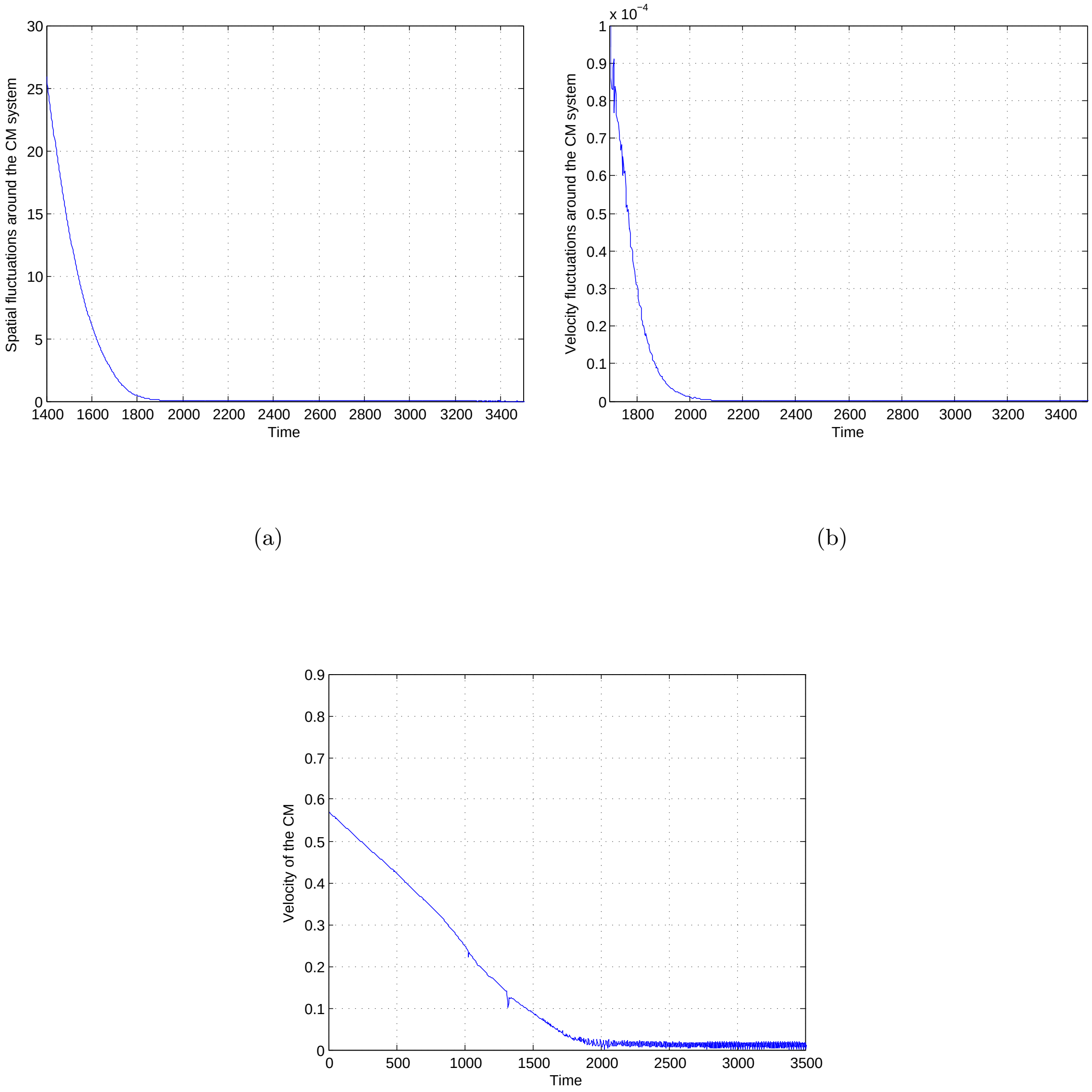

(a) (b)

(c)

Figure 6.4. **Test 3**. (a)-(b) Spatial and velocity fluctuations around the centre of mass system: $Fl_X(t)$ and $Fl_V(t)$. For $t \geq 3109$ $Fl_X(t)$ and $Fl_V(t)$ are less than 10^{-10} (on the x-axis only a part of the time domain is shown). (c) Norm of the velocity of the centre of mass $\|\mathbf{V}_{\mathrm{CM}}(t)\|$ versus time. For $t \geq 2579$ this velocity is less than 1.87×10^{-2}.

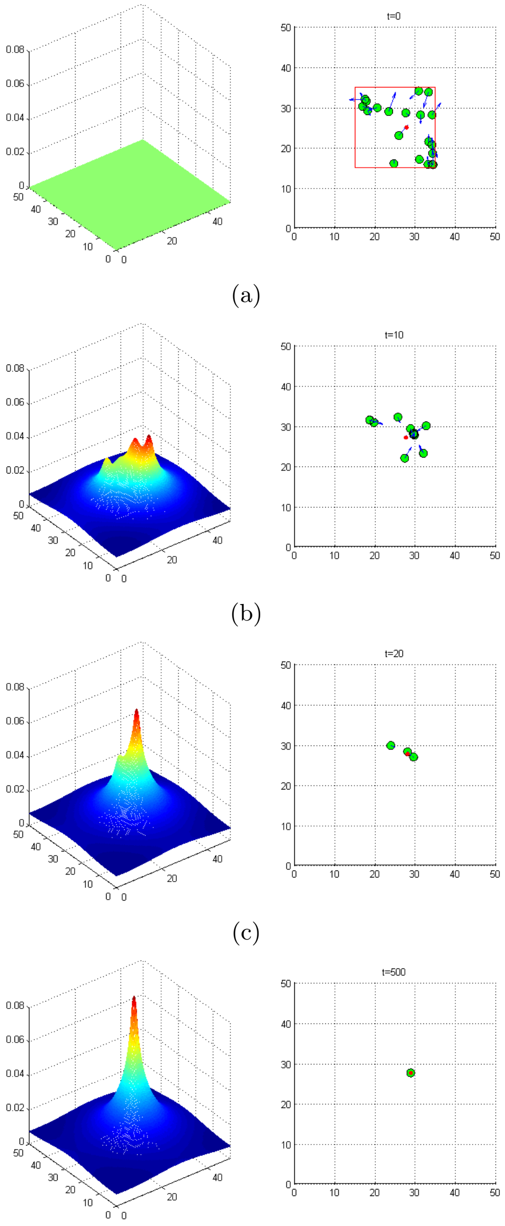

(a)

(b)

(c)

(d)

Figure 6.5. **Test 4**. Numerical simulation in a spatial domain $\Omega = [0, 50] \times [0, 50]$ with periodic boundary conditions, and in the time interval $[0, 500]$. The parameters values are $\sigma = 0.5$, $\beta = 5$, $\gamma = 2 \times 10^2$, $D = 2 \times 10^2$, $\xi = 0.5$, $V_{0,\max} = 3$, and $\mathbf{X}_0$ randomly taken in the red square shown in (a). Spatial and temporal discretizations are respectively $\Delta x = \Delta y = 0.25$ and $\Delta t = 10^{-4}$. The four plots are respectively at time steps $t = 0, 10, 30, 500$. The chemoattractant concentration $f(\mathbf{x}, t)$ is on the left, while on the right there is the positions and the velocities of the particles. The red marker marks the centre of mass of the system, and the blue arrows are the velocity vectors.

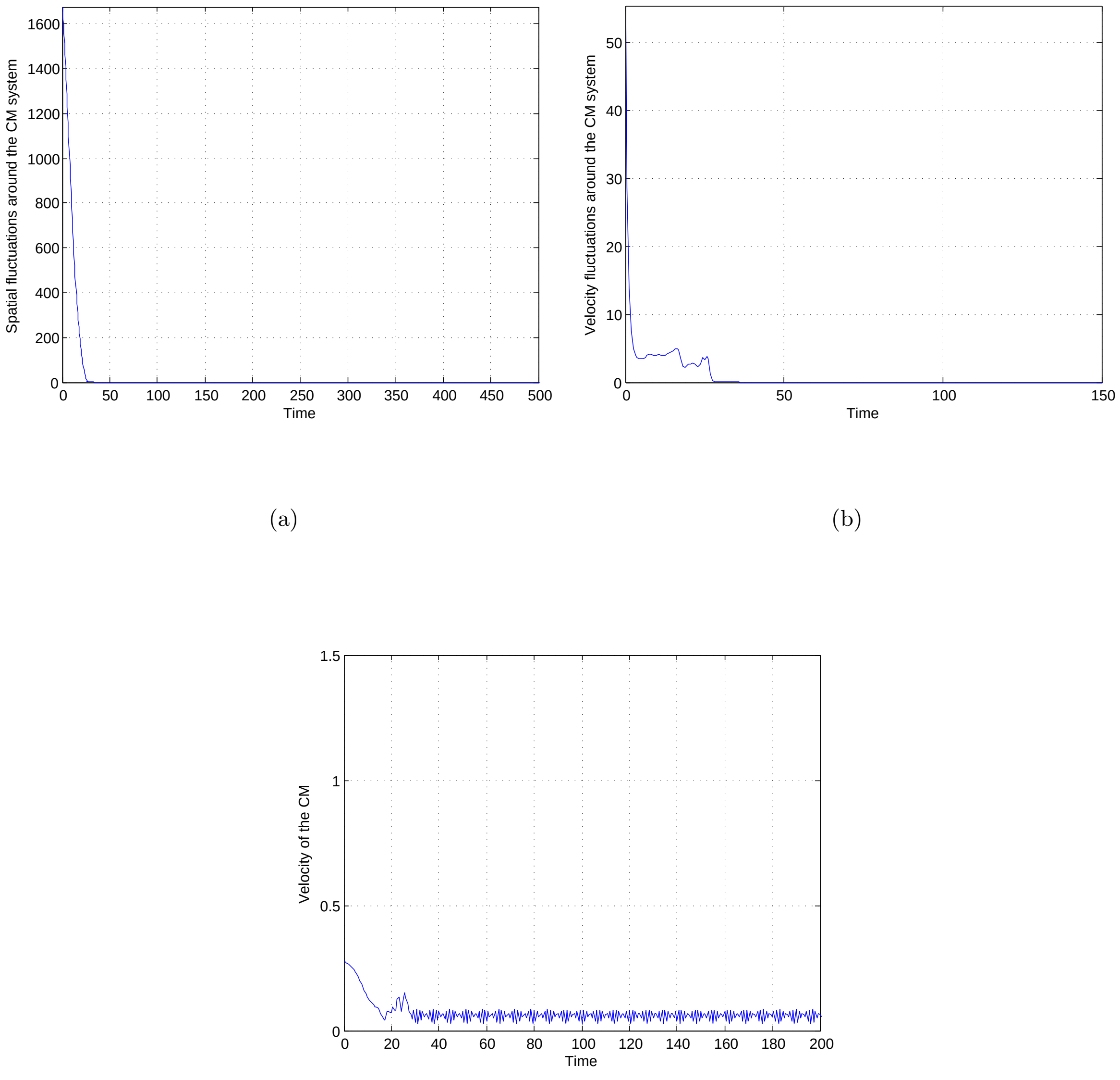

(a)

(b)

(c)

FIGURE 6.6. **Test 4**. (a)–(b) Spatial and velocity fluctuations around the centre of mass system $Fl_X(t)$ and $Fl_V(t)$ (x-axis shows only a part of the time domain). For $t \geq 34$ we have values less than 10^{-10}. (c) Norm of the velocity of the centre of mass $\|\mathbf{V}_{\mathrm{CM}}(t)\|$ versus time (only a part of the time interval is shown on the x-axis). For $t \geq 28$ this velocity is less than 8.39×10^{-2}.

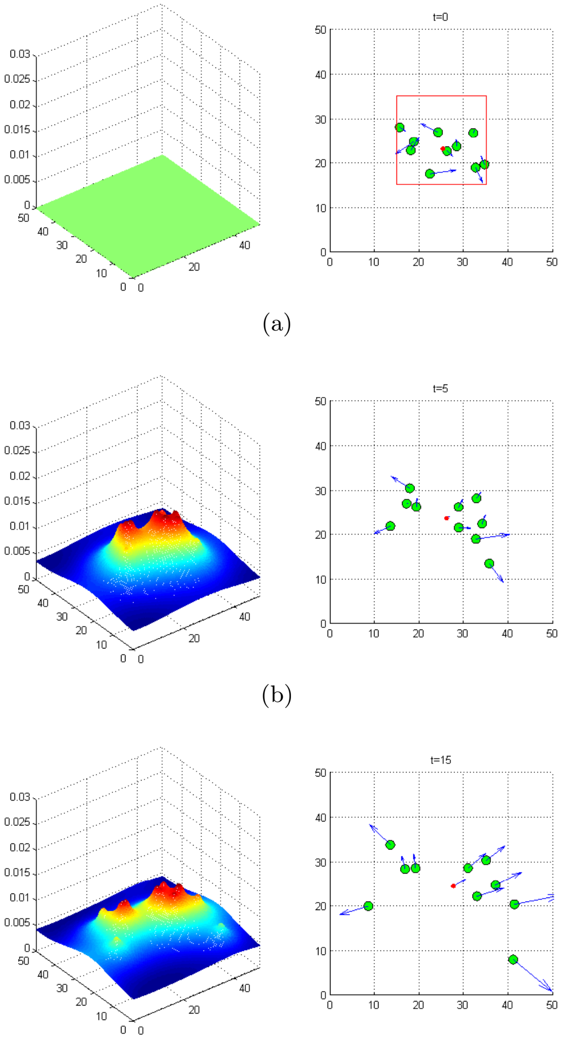

(a)

(b)

(c)

Figure 6.7. **Test 5**. Numerical simulation in a spatial domain $\Omega = [0, 50] \times [0, 50]$ with periodic boundary conditions, and in the time interval $[0, 15]$. The parameters values are $\sigma = 0.8$, $\beta = 5$, $\gamma = 0$, $D = 2 \times 10^2$, $\xi = 0.5$, $V_{0,\max} = 3$, and $\mathbf{X}_0$ randomly taken in the red square shown in (a). Spatial and temporal discretizations are respectively $\Delta x = \Delta y = 0.25$ and $\Delta t = 10^{-4}$. The red marker indicates the centre of mass of the system, and the blue arrows are the velocity vectors. On the left there is the chemoattractant concentration, while on the right the positions and the velocities of the particles. In this case the motion equations and the chemoattractant equation are decoupled and for the particles we simulate the pure Cucker-Smale model (1.1). Taken into account the parameters values and the initial data the flocking behaviour is not ensured by results in Ha and Liu (2009). In fact, from the three plots, taken respectively at time steps $t = 0, 5, 15$, we can observe a dispersion of the initial group.

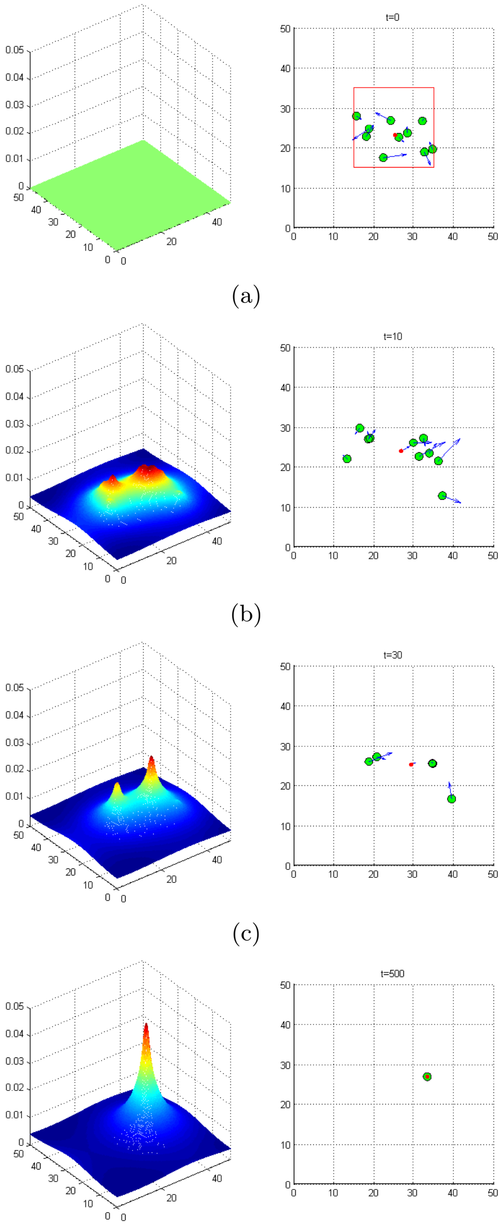

(a)

(b)

(c)

(d)

Figure 6.8. **Test 6**. Numerical simulation in a spatial domain $\Omega = [0, 50] \times [0, 50]$ with periodic boundary conditions, and in the time interval $[0, 500]$. The parameters values and the initial data are as in Figure 6.7: $\sigma = 0.8$, $\beta = 5$, $D = 10^2$, $\xi = 0.5$, $V_{0,\max} = 3$, and $\mathbf{X}_0$ as in Figure 6.7 (a). Then here a nonzero value for γ is chosen: $\gamma = 2 \times 10^2$. Spatial and temporal discretizations are $\Delta x = \Delta y = 0.25$ and $\Delta t = 10^{-4}$. The four plots are respectively at time steps $t = 0, 10, 30, 500$. On the left there is the chemoattractant concentration $f(\mathbf{x}, t)$, while on the right the positions and the velocities of the particles. The red marker is the centre of mass of the system, and the blue arrows are the velocity vectors. Comparing this figure with Figure 6.7, we observe that, introducing the chemotactic effect, the time-asymptotic convergence of the particles is recovered.

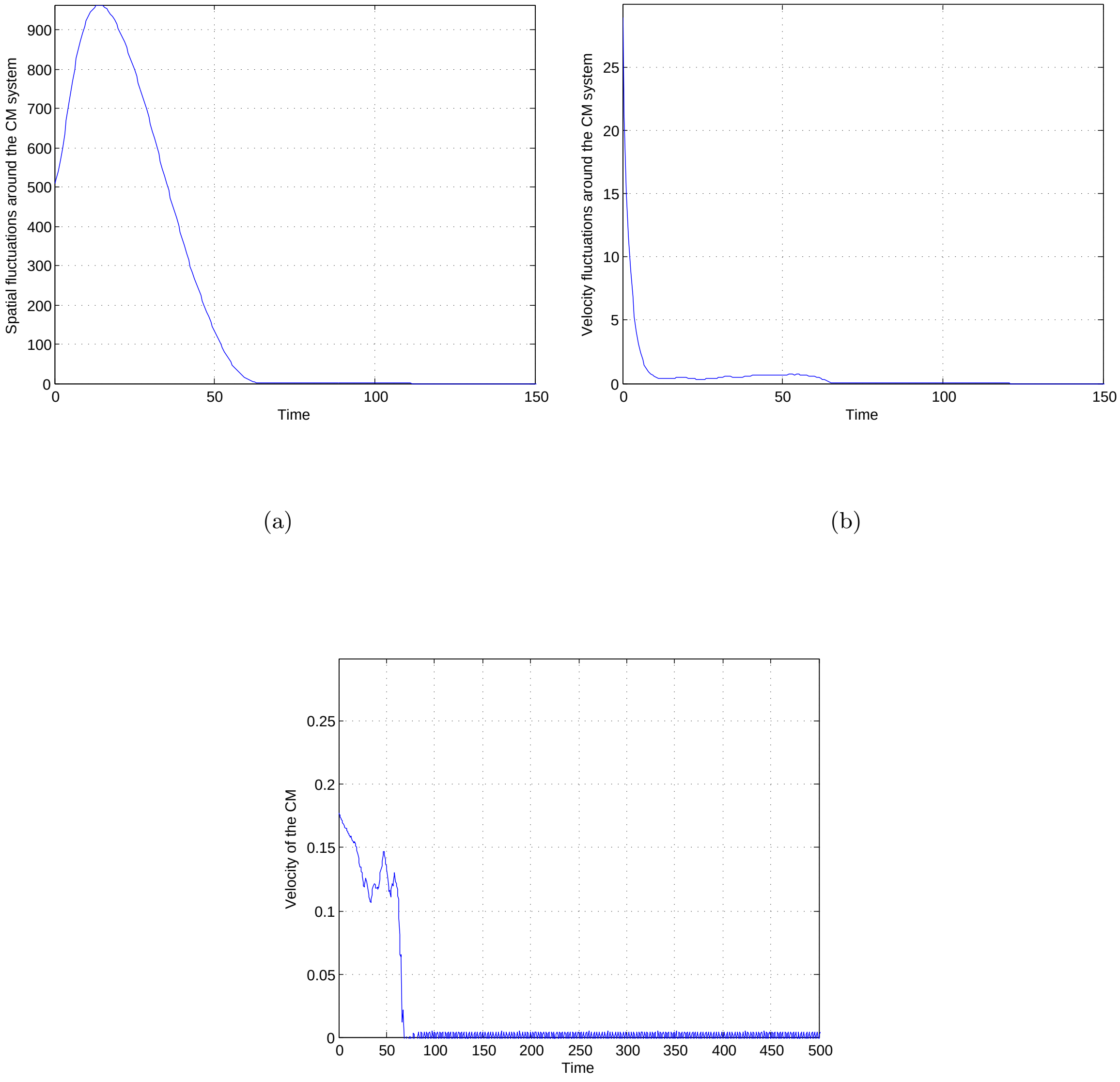

(a) (b)

(c)

Figure 6.9. **Test 6**. (a)-(b) Spatial fluctuation $Fl_X(t)$ and velocity fluctuation $Fl_V(t)$ around the centre of mass system as a function of the time (x-axis shows only a part of the time interval). For $t \geq 107$ $Fl_X(t)$ and $Fl_V(t)$ are less than 10^{-10} (on the x-axis only a part of the time domain is shown). (c) Velocity of the centre of mass $\|\mathbf{V}_{\mathrm{CM}}(t)\|$ versus time. For $t \geq 65$ we have values smaller than 2.1×10^{-2}.

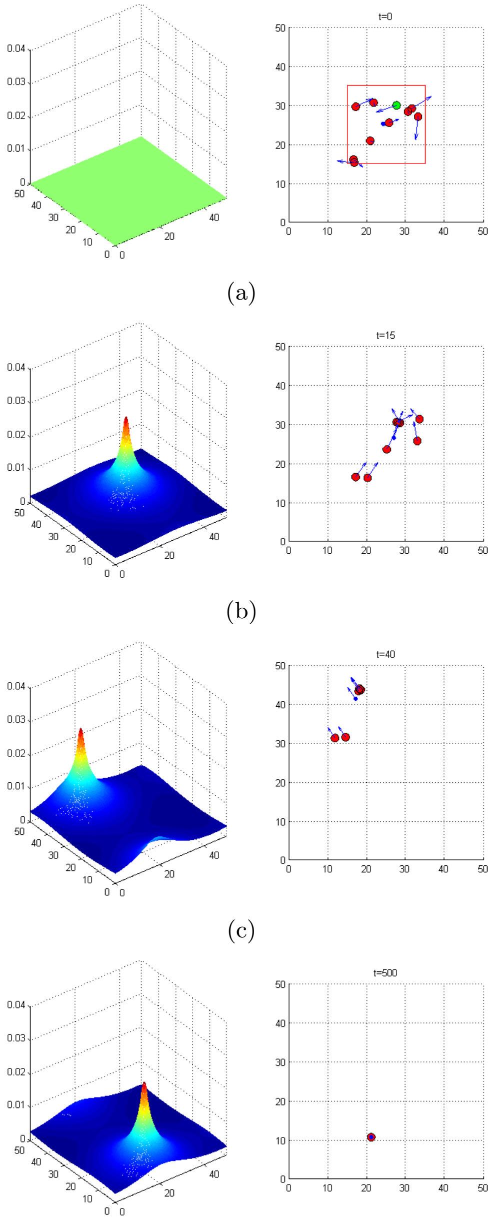

(a)

(b)

(c)

(d)

FIGURE 6.10. **Test 7**. Numerical simulation in a spatial domain $\Omega = [0, 50] \times [0, 50]$ with periodic boundary conditions, and in the time interval $[0, 500]$. The parameters values are $\sigma = 0.5$, $\beta = 5$, $\gamma = 1.5 \times 10^2$, $D = 2 \times 10^2$, $\xi = 3$, $V_{0,\max} = 0.3$, and $\mathbf{X}_0$ randomly taken in the red square shown in (a). Spatial and temporal discretizations are respectively $\Delta x = \Delta y = 0.25$ and $\Delta t = 10^{-4}$. The green cell marks a leader cell (●), that produce the chemical signal, while the other red cells are the followers (●), that do not produce any signal and follow the chemoattractant gradient. The blue marker is the centre of mass of the system, and the blue arrows are the velocity vectors. The four plots are respectively at time steps $t = 0, 15, 40, 500$. On the left there is the chemoattractant concentration, while on the right the positions and the velocities of the particles.

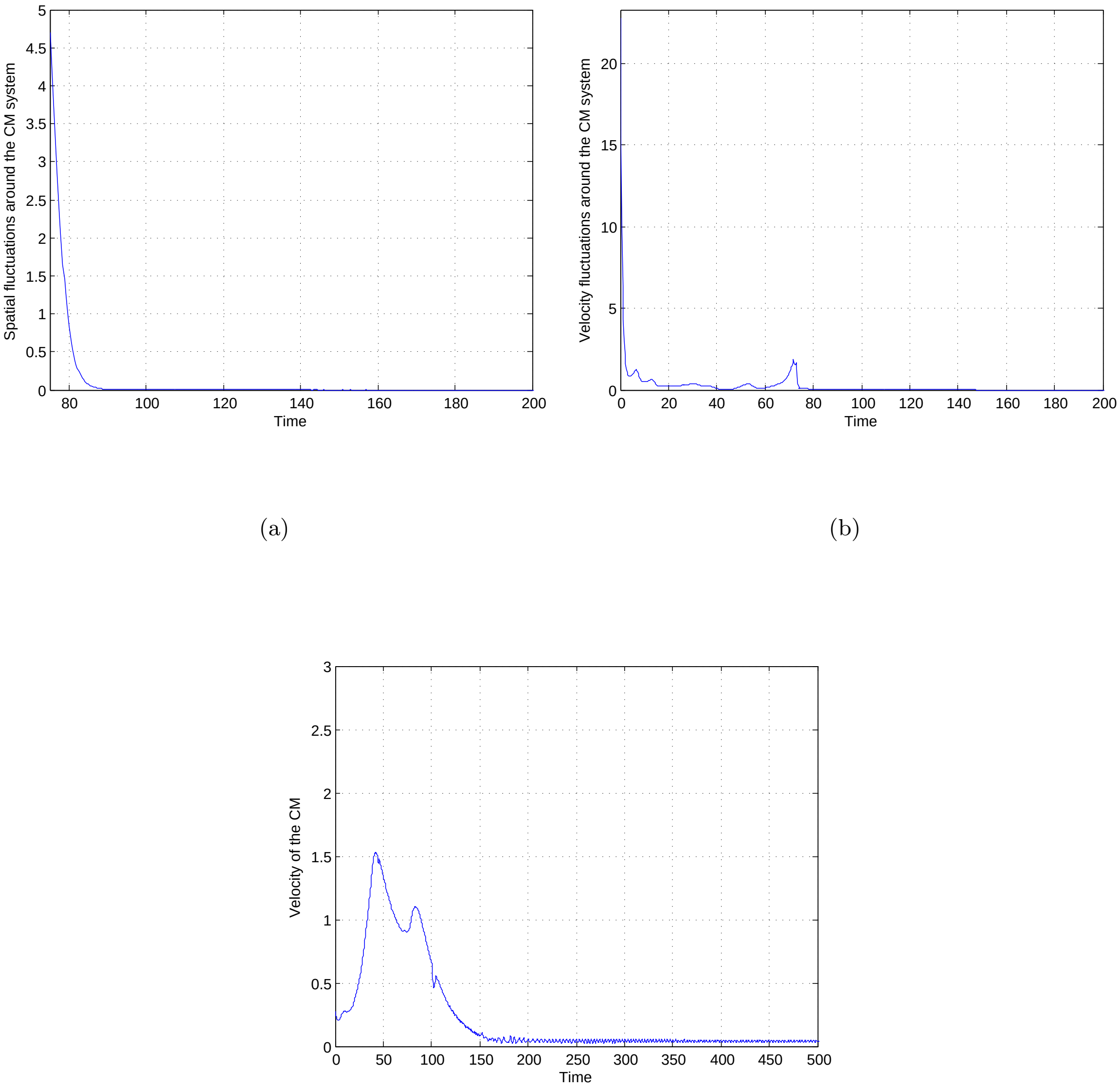

(a)

(b)

(c)

FIGURE 6.11. **Test 7**. (a)-(b) Spatial and velocity fluctuations, $Fl_X(t)$ and $Fl_V(t)$, around the centre of mass system (only a part of the time domain is shown on the x-axis). For $t \geq 131$ $Fl_X(t)$ and $Fl_V(t)$ are less than 10^{-10}. (c) Velocity of the centre of mass $\|\mathbf{V}_{\mathrm{CM}}(t)\|$ as a function of the time. For $t \geq 328$ we have values smaller than 5.3×10^{-2}.

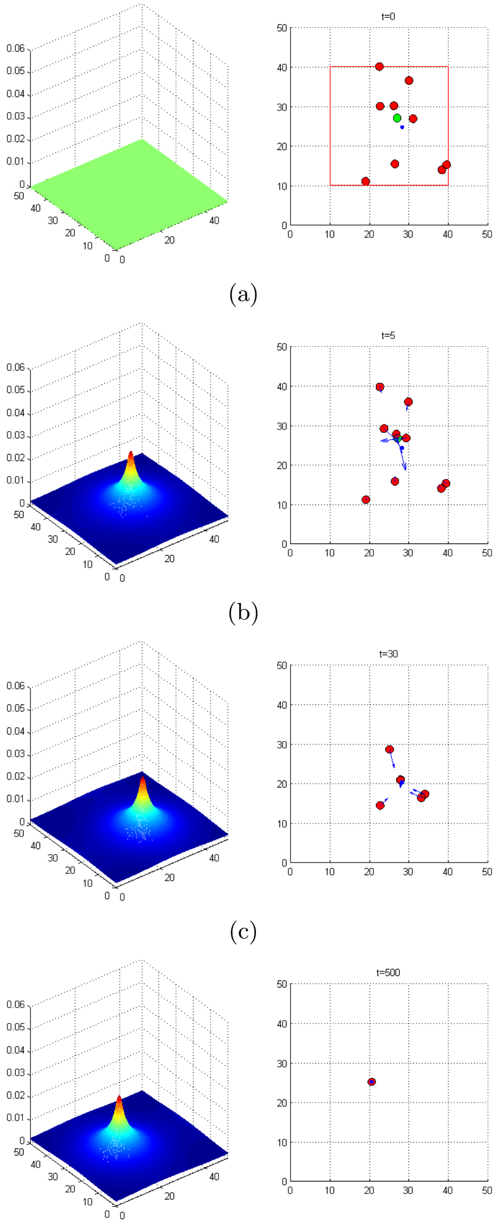

(a)

(b)

(c)

(d)

Figure 6.12. **Test 8**. Numerical simulation in a spatial domain $\Omega = [0, 50] \times [0, 50]$ with periodic boundary conditions, and in the time interval $[0, 500]$. Spatial and temporal discretizations are respectively $\Delta x = \Delta y = 0.25$ and $\Delta t = 10^{-4}$. In this case we fix a zero initial velocity, $V_{0,\max} = 0$, and the parameters $\sigma = 0.6$, $\beta = 2$, $\gamma = 10^2$, $D = 2 \times 10^2$, $\xi = 3$, and $\mathbf{X}_0$ randomly taken in the red square shown in (a). As in Figure 6.10 we consider a single leader cell (●) and other red follower cells (●). Because of the zero initial velocity, if we considered the pure Cucker-Smale (1.1), we would have all particles constant in time in the initial position. Conversely, in the four plots at time steps $t = 0, 5, 30, 500$ we observe the time-asymptotic convergence of the migrating group.

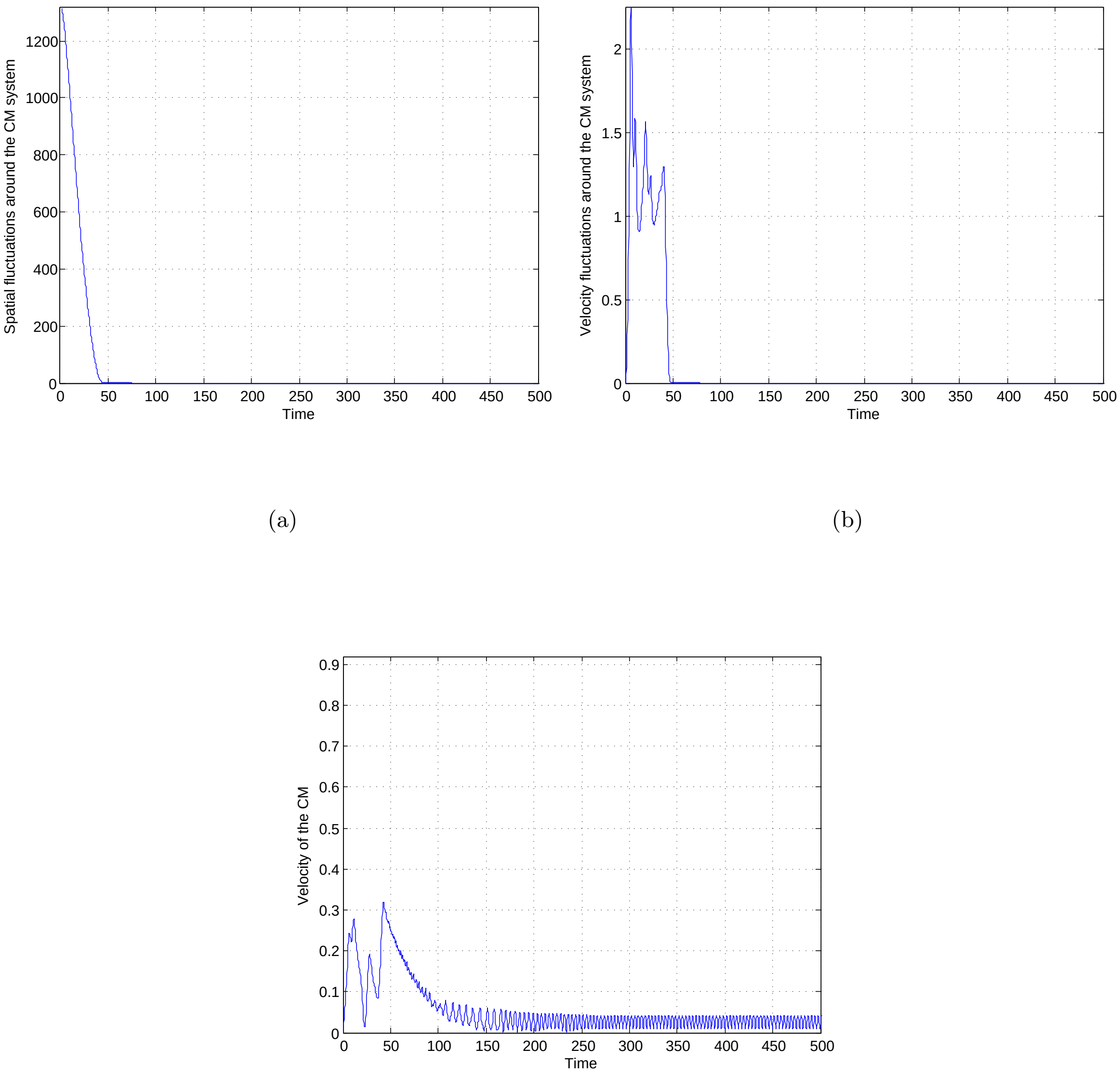

(a)

(b)

(c)

Figure 6.13. **Test 8**. (a)-(b) Spatial and velocity fluctuations around the centre of mass system as a function of the time: $Fl_X(t)$ and $Fl_V(t)$. For $t \geq 67$ $Fl_X(t)$ and $Fl_V(t)$ are less than 10^{-10}. (c) Velocity of the centre of mass $\|\mathbf{V}_{\mathrm{CM}}(t)\|$ versus time. For $t \geq 109$ this quantity is smaller than 4.3×10^{-2}.

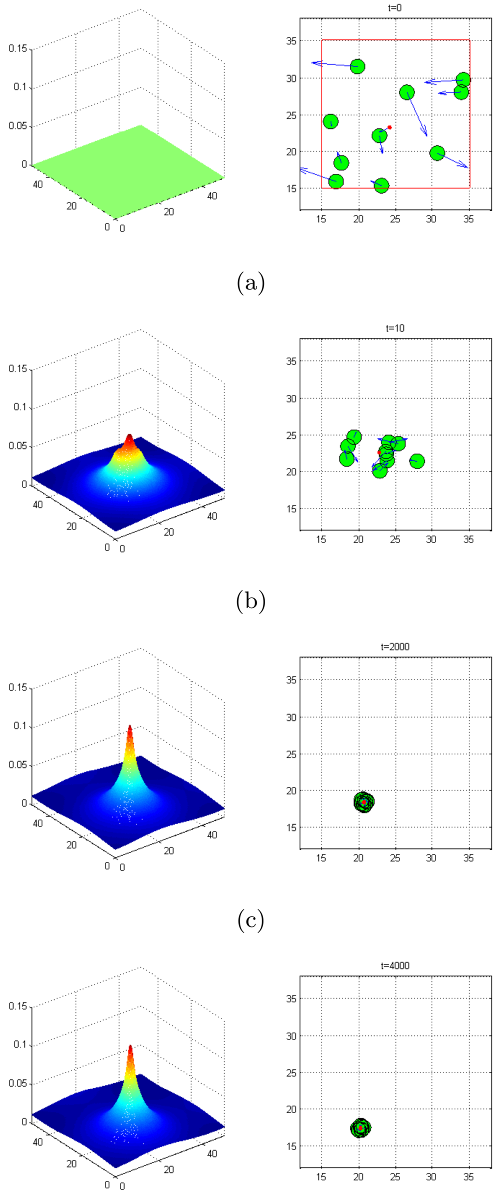

(a)

(b)

(c)

(d)

Figure 6.14. **Test 9**. Numerical simulation in a spatial domain $\Omega = [0, 50] \times [0, 50]$ with periodic boundary conditions, and in the time interval $[0, 4000]$ (plots on the right shown only a part of the spatial domain). Spatial and temporal discretizations are respectively $\Delta x = \Delta y = 0.25$ and $\Delta t = 10^{-4}$. In this test only the chemotactic force is considered, neglecting the alignment effect ($\beta = 0$). For the other values we fix $\gamma = 10^2$, $D = 2 \times 10^2$, $\xi = 1.5$, $V_{0,\max} = 0.8$, and $\mathbf{X}_0$ randomly taken in the red square shown in (a). The plots taken at time steps $t = 0, 10, 2000, 4000$ display the aggregation of the initial group of particles. In this case the convergence is not observed, but an oscillating behaviour around their centre of mass is shown.

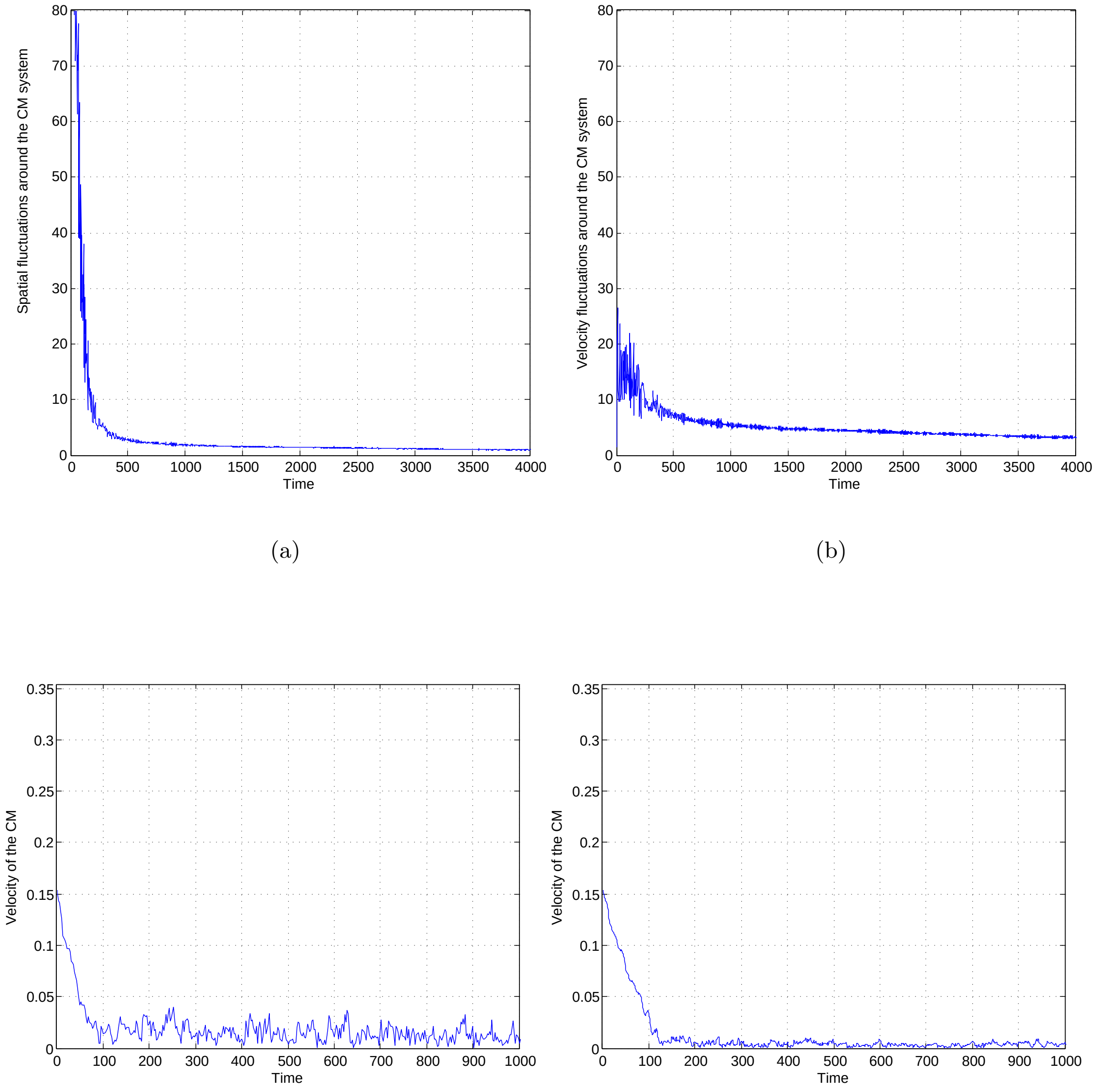

(a) (b)

(c) (d)

FIGURE 6.15. **Test 9**. (a)-(b) Spatial and velocity fluctuations, $Fl_X(t)$ and $Fl_V(t)$, around the centre of mass system versus time (only a part of the time domain is shown on the x-axis). In this case $Fl_X(t)$ and $Fl_V(t)$ remain bounded but do not converge to zero. In particular we have $Fl_X(t) \geq 0.88$ and, if we consider a trend line, its slope seems to decrease monotonically. In particular in the time intervals $[0, 800]$ and $[3200, 4000]$, the slope of the fit line changes from -1.46×10^{-1} to -1.84×10^{-4}. (c) Velocity of the centre of mass $\|\mathbf{V}_{\mathrm{CM}}(t)\|$ versus time, using a spatial and a temporal discretization given by $\Delta x = \Delta y = 2.5$ and $\Delta t = 10^{-4}$ (x-axis shows a part of the time interval). For $t \geq 254$ this quantity is smaller than 3.79×10^{-2}. (d) With a finer mesh, $\Delta x = \Delta y = 0.125$ and $\Delta t = 10^{-5}$, we obtain smaller values: for $t \geq 120$ we have values less than 1.41×10^{-2}.

7. Conclusions

In this paper we have proposed an extension of the Cucker-Smale model introducing a mathematical model for collective motion driven by an alignment and a chemotaxis effect. We have adopted a hybrid description, discrete for the particles and for the motion equations, and continuous for the molecular level, containing the equation for the chemical signal.

We have studied our model by both an analytical and a numerical point of view. By the analytical point of view, using a fixed–point theorem, we have proved local existence and uniqueness of the solution of the nonlinear system. Then, through a principle of continuation of solutions, we have extended such result proving global existence and uniqueness for all times. Moreover, we have investigated the asymptotic behaviour of particular equilibrium configurations, corresponding to a state in which all particles are located in a same position with zero velocity. On the linearized system around such configurations we have proved, using a Lyapunov functional approach, the asymptotic convergence of the particles in their centre of mass with same velocity. Then the velocity of the centre of mass is proved to go time-asymptotically to zero. By a numerical point of view this property has been tested on the nonlinear system, finding a complete concordance with the analytical results, and some numerical simulations have been proposed. Among these, we have discussed the competition between alignment and chemotactic effects varying the parameters of the system. We have found a decay in the rate of convergence of the particles when the strength of the alignment term increases with respect to the chemotaxis. On the other hand, a growth in the rate of convergence can be found with the same parameters and with a greater number of interacting particles. Then we have considered the presence of two cell populations, inspired from the model for the zebrafish lateral line proposed in Di Costanzo et al (2015), finding the convergence of cells towards the sources of chemical signal. Finally, the case of a pure chemotactic effect, without alignment, has been simulated. Numerical results have shown the absence of convergence in the migrating group, suggesting that our model, with the only chemotaxis mechanism, is not able to describe biological processes leading to stationary aggregates.

Future perspectives can concern the extension of the stability result, proved on the linearized system, to the full nonlinear model. Furthermore, other interactions could be taken into account in the collective motion, such as adhesion-repulsion, damping or lateral inhibition terms, similar to those introduced in the aforesaid paper on the zebrafish primordium. This would be interesting in view of studying, in an analytical framework, the morphogenetic process arising in the lateral line development, and establish results in relation to the neuromast formation and deposition.

Appendix A. Numerical approximation

The numerical approximation scheme used in the dynamical tests employs a 2D finite difference method on a spatial domain $\Omega := [a, b] \times [c, d]$ with periodic boundary conditions. If Δx and Δy are the spatial steps and Δt the time step, we define the grid points (x_m, y_n, t_k), where $x_m = m\Delta x$, $x_n = n\Delta y$ and $t_k = k\Delta t$. The notation $u^k_{m,n}$ will denote the approximation of a function $u(x, y, t)$ at the grid point (x_m, y_n, t_k).

For the parabolic equation $(6.1)_3$, in order to eliminate the stiff term $-f$ we perform the exponential transformation

$$f(\mathbf{x}, t) = e^{-t} u(\mathbf{x}, t),$$

where $u(\mathbf{x},t)$ satisfies the equation

$$\partial_t u = D\Delta u + e^t \xi \sum_{j=1}^{N} \chi_{\mathbf{B}(\mathbf{X}_j,1)}, \tag{A.1}$$

with initial condition

$$u(\mathbf{x},0)=0,$$

and periodic boundary conditions.

Now, for (A.1) we apply a central difference scheme in space and the parabolic Crank-Nicolson scheme in time. Namely we write

$$\begin{aligned}\frac{u^{k+1}_{m,n}-u^k_{m,n}}{\Delta t} &= \frac{D}{2}\left(D^2_x u^{k+1} + D^2_y u^{k+1}\right) + \frac{D}{2}\left(D^2_x u^{k} + D^2_y u^{k}\right)\\ &+ \frac{1}{2}e^{(k+1)\Delta t}\xi \sum_{j=1}^{N}\chi_{\mathbf{B}(\mathbf{X}^k_j,1)}\\ &+ \frac{1}{2}e^{k\Delta t}\xi \sum_{j=1}^{N}\chi_{\mathbf{B}(\mathbf{X}^k_j,1)},\end{aligned}$$

where the second finite differences $D^2_x u$ and $D^2_y u$ are given by

$$\begin{aligned} D^2_x u^k &:= \frac{u^k_{m-1,n} - 2u^k_{m,n} + u^k_{m+1,n}}{\Delta x^2},\\ D^2_y u^k &:= \frac{u^k_{m,n-1} - 2u^k_{m,n} + u^k_{m,n+1}}{\Delta y^2},\end{aligned} \tag{A.2}$$

and

$$\chi_{\mathbf{B}(\mathbf{X}^k_j,1)} = \begin{cases} 1, & \text{if } \quad (x_m,y_n)\in \mathbf{B}(\mathbf{X}^k_j,1);\\ 0, & \qquad \text{otherwise.}\end{cases}$$

For equations $(6.1)_1$ we adopt a one step IMEX method, putting in implicit the term depending on the velocities and in explicit the gradient term (Hundsdorfer and Verwer, 2003). The scheme reads:

$$\begin{cases} \dfrac{\mathbf{V}^{k+1}_i - \mathbf{V}^k_i}{\Delta t} &= \dfrac{\beta}{N}\displaystyle\sum_{j=1}^{N} \frac{1}{\left(1+\left\|\mathbf{X}^k_i-\mathbf{X}^k_j\right\|^2\right)^\sigma}(\mathbf{V}^{k+1}_j - \mathbf{V}^{k+1}_i) + \gamma \mathcal{I}_{\mathbf{X}^k_i}\left(\nabla_{m,n} f^k\right),\\ \\ \dfrac{\mathbf{X}^{k+1}_i - \mathbf{X}^k_i}{\Delta t} &= \mathbf{V}^k_i,\end{cases} \tag{A.3}$$

where

$$\nabla_{m,n} f^k := \left(\frac{f^k_{m+1,n} - f^k_{m,n}}{2\Delta x}, \frac{f^k_{m,n+1} - f^k_{m,n}}{2\Delta y}\right),$$

and $\mathcal{I}_{\mathbf{X}^k_i}(\nabla_{m,n} f^k)$ represents an interpolation of the values $\nabla_{m,n} f^k$ on the grid points nearest to $\mathbf{X}^k_i$.

About the spatial and temporal steps employed in the simulations we chose $\Delta x = \Delta y$ and, in the first time steps, the parabolic CFL condition $\Delta t \sim \frac{\Delta x^2}{D}$, which has shown more stability in the numerical tests, taken into account in (A.1) the discontinuous source term and the value of $u(\mathbf{x}, t)$ initially near to zero. In practice, after few time steps, we have release the parabolic CFL in favour of $\Delta t \sim \Delta x$.

References

Albi G, Pareschi L (2013) Modeling self-organized systems interacting with few individuals: From microscopic to macroscopic dynamics. Appl Math Lett 26(4):397–401

Aoki I (1982) A simulation study on the schooling mechanism in fish. Bullettin Of The Japanese Society Scientific Fischeries 48(8):1081–1088

Arboleda-Estudillo Y, Krieg M, Stühmer J, Licata NA, Muller DJ, Heisenberg CP (2010) Movement Directionality in Collective Migration of Germ Layer Progenitors. Curr Biology 20:161–169

Ballerini M, Cabibbo N, Candelier R, Cavagna A, Cisbani E, Giardina I, Lecomte V, Orlandi A, Parisi G, Procaccini A, Viale M, Zdravkovic V (2008) Interaction ruling animal collective behavior depends on topological rather than metric distance: Evidence from a field study. P Natl Acad Sci USA 105(4):1232–1237

Belmonte JM, Thomas GL, Brunnet LG, de Almeida RM, Chaté H (2008) Self-propelled particle model for cell-sorting phenomena. Phys Rev Lett 100(24):248702

Bruno L, Tosin A, Tricerri P, Venuti F (2011) Non-local first-order modelling of crowd dynamics: A multidimensional framework with applications. Applied Mathematical Modelling 35:426–445

Burton TA (2005) Volterra Integral and Differential Equations. Second Edition. Springer

Carrillo JA, Fornasier M, Rosado J, Toscani G (2010) Asymptotic Flocking Dynamics for the Kinetic Cucker-Smale Model. SIAM J Math Anal 42(1):218–236

Colin T, Durrieu MC, Joie J, Lei Y, Mammeri Y, Poignard C, Saut O (2013) Modeling of the migration of endothelial cells on bioactive micropatterned polymers. Math BioSci and Eng 10(4):997–1015

Couzin ID, Krause J, James R, Ruxton GD, Franks NR (2002) Collective memory and spatial sorting in animal groups. J Theor Biol 71:1–11

Couzin ID, Krause J, Franks NR, Levin SA (2005) Effective leadership and decision-making in animal groups on the move. Nature 433:513–516

Cristiani E, Piccoli B, Tosin A (2010) Modeling self-organization in pedestrians and animal groups from macroscopic and microscopic viewpoints. In: Naldi G, Pareschi L, Toscani G (eds) Mathematical modeling of collective behavior in socio-economic and life-sciences, Modeling and Simulation in Science, Engineering, and Technology, Birkhäuser Boston, pp 337–364

Cristiani E, Frasca P, Piccoli B (2011) Effects of anisotropic interactions on the structure of animal groups. J Math Biol 62:569–588

Cristiani E, Piccoli B, Tosin A (2014) Multiscale Modeling of Pedestrian Dynamics, MS&A: Modeling, Simulation and Applications, vol 12. Springer International Publishing

Cristiani E, Priuli FS, Tosin A (2015) Modeling rationality to control self-organization of crowds: an environmental approach. SIAM J Appl Math 75:605–629

Cucker F, Dong JG (2010) Avoiding collisions in flocks. IEEE Transactions on Automatic Control 55:1238–1243

Cucker F, Dong JG (2011) A General Collision-Avoiding Flocking Framework. IEEE Transactions on Automatic Control 56(5):1124–1129

Cucker F, Huepe C (2008) Flocking with informed agents. MathematicS In Action 1:1–25

Cucker F, Mordecki E (2008) Flocking in noisy environments. J Math Pures Appl 89:278–296

Cucker F, Smale S (2007) Emergent Behavior in Flocks. Ieee T Automat Contr 52(5):852–862

Di Costanzo E, Natalini R, Preziosi L (2015) A hybrid mathematical model for self-organizing cell migration in the zebrafish lateral line. J of Math Biol 71:171–214

D'Orsogna MR, Chuang YL, Bertozzi AL, Chayes LS (2006) Self-Propelled Particles with Soft-Core Interactions: Patterns, Stability, and Collapse. Phys Rev Lett 96(10):104302

Eisenbach M, Lengeler JW (2004) Chemotaxis. Imperial College Press

Faria JJ, Dyer JRG, Tosh CR, Krause J (2010) Leadership and social information use in human crowds. Animal Behaviour 79(4):895–901

Fish FE (1995) Kinematics of ducklings swimming in formation: consequences of position. Journal of Experimental Zoology 273:1–11

Grégoire G, Chaté (2004) Onset of collective and cohesive motion. Phys Rev Lett 92:025702

Grégoire G, Chaté H, Tu Y (2003) Moving and staying together without a leader. Physica D 181:157

Ha SY, Levy D (2009) Particle, kinetic and fluid models for phototaxis. Discrete and Continuous Dynamical Systems - Series B 12(1):77–108

Ha SY, Liu JG (2009) A simple proof of the Cucker-Smale flocking dynamics and mean-field limit. Commun Math Sci 7(2):297–325

Ha SY, Lee K, Levy D (2009) Emergence of time-asymptotic flocking in a stochastic Cucker-Smale system. Comm Math Sci 7(2):453–469

Hatzikirou H, Deutsch A (2007) Collective guidance of collective cell migration. Curr Top Dev Biol 81:401–434

Helbing D, Schweitzer F, Keltsch J, Molnár P (1997) Active walker model for the formation of human and animal trail systems. Physical Review 56(3):2527–2539

Hemelrijk CK, Hildenbrandt H (2008) Self-organized shape and frontal density of fish schools. Ethology 114:245–254

Hundsdorfer W, Verwer JG (2003) Numerical Solution of Time-Dependent Advection-Diffusion-Reaction Equations. Computational Mathematics, Springer

Huth A, Wissel C (1992) The simulation of the movement of fish schools. J Theor Biol 156:365–385

Ioannou CC, Tosh CR, Neville L, Krause J (2008) The confusion effect. from neural networks to reduced predation risk. Behavioral Ecology 19(1):126–130

Jadbabaie A, Lin J, Morse A (2003) Coordination of groups of mobile autonomous agents using nearest neighbor rules. IEEE Trans Autom Control 48(6):988–1001

Joie J, Lei Y, Colin T, Durrieu MC, Poignard C, Saut O (2013) Modelling of migration and orientation of endothelial cells on micropatterned polymers. Research Report RR-8252, Inria Institute, URL `https://hal.inria.fr/hal-00795238`

Khalil HK (2002) Nonlinear Systems. Third Edition. Prentice Hall

Lakshmikantham V, Rama MRM (1995) Theory of integro-differential equations, Stability and Control: Theory, Methods and Applications, vol 1. Gordon and Breach Science Publishers

Méhes E, Vicsek T (2014) Collective motion of cells: from experiments to models. Integr Biol 6(9):831–854

Moussaïd M, Helbing D, Theraulaz G (2011) How simple rules determine pedestrian behavior and crowd disasters. Proceeding of the National Academy of Sciences of the United States of America 108:6884–6888

Murray JD (2003) Mathematical biology II: Spatial Models and Biomedical Applications. Third edition. Springer

Naldi G, Pareschi L, Toscani G (eds) (2010) Mathematical modeling of collective behavior in socio-economic and life-sciences. Modeling and Simulation in Science, Engineering, and Technology, Birkhäuser Boston

Pareschi L, Toscani G (2014) Interacting Multiagent Systems: Kinetic Equations and Monte Carlo Methods. Oxford University Press

Perthame B (2007) Transport equations in biology. Birkhäuser

Piccoli B, Tosin A (2009) Pedestrian flows in bounded domains with obstacles. Contin Mech Thermodyn 21(2):85–107

Pitcher T, Magurran A, Winfield I (1982) Fish in larger shoals find food faster. Behav Ecol and Sociobiology 10(2):149–151

Sepúlveda N, Petitjean L, Cochet O, Grasland-Mongrain E, Silberzan P, Hakim V (2013) Collective Cell Motion in an Epithelial Sheet Can Be Quantitatively Described by a Stochastic Interacting Particle Model. PLOS Computational Biology 9(3):e1002944

Strömbom D (2011) Collective motion from local attraction. J Theor Biol 283:145–151

Szabò B, Szöllösi GJ, Gönci B, Jurànyi Z, Selmeczi D, Vicsek T (2006) Phase transition in the collective migration of tissue cells: Experiment and model. Phys Rev E 74(6):061908

Tsitsiklis J (1984) Problems in decentralized decision making and computation. Ph.D. dissertation. Dept. of Electrical Engineering and Computer Science, Massachusetts Institute of Technology, Cambridge, MA

Vicsek T, Zafeiris A (2012) Collective motion. Physics Reports 517(3):71–140

Vicsek T, Cziròk A, Ben-Jacob E, Cohen I, Shochet O (1995) Novel Type of Phase Transition in a System of Self-Driven Particles. Phys Rev Lett 75(6):1226–1229

Wazwaz AM (2011) Linear and Nonlinear Integral Equations. Methods and Applications. Springer